

Water-energy nexus: A thermoeconomic analysis of polygeneration systems for small Mediterranean islands



Francesco Calise^a, Francesco Liberato Cappiello^a, Maria Vicidomini^{a,*},
Fontina Petrakopoulou-Robinson^b

^a Department of Industrial Engineering, University of Naples Federico II, Naples, Italy

^b Department of Thermal and Fluid Engineering, Universidad Carlos III de Madrid, Spain

ARTICLE INFO

Keywords:

PV
CPVT
Solar desalination
RO
MED
Polygeneration

ABSTRACT

This paper focuses on the energy-water nexus, aiming at developing novel systems producing simultaneously energy and water. This work investigates two solar polygeneration plants for the production of thermal and cooling energy, electricity, and desalinated water for two small Mediterranean islands. In this case, seawater and solar energy are largely available, whereas freshwater is scarce and extremely expensive. The work also aims to compare different technologies included in the polygeneration systems. In particular, the first plant is based on concentrating photovoltaic/thermal solar collectors, producing electric and thermal energy. The thermal energy is used to produce space heating, domestic hot water and space cooling by means a single-stage Lithium Bromide/Water absorption chiller. An electric auxiliary chiller is also included. A multi-effect distillation unit is included for freshwater production supplied by the concentrating photovoltaic/thermal collectors solar energy and an auxiliary biomass-fired heater. In the second plant, a photovoltaic field is coupled with electric driven technologies, such as heat pumps for space heating, cooling and domestic hot water production and a reverse osmosis unit. The solar electrical energy excess is delivered to the grid. The third polygeneration plant includes the same components as the first layout but it is equipped with a reverse osmosis unit. Two main case studies, Favignana and Salina islands (South Italy) are selected. The heating, cooling and electric hourly loads of some buildings located in both investigated weather zones are calculated in detail. In particular, space heating and cooling loads are calculated by means of the Type 56 of TRNSYS (version 17), coupled to the Google SketchUp TRNSYS3d plug-in. The buildings geometry, envelope, windows, lighting, machineries heat gains schedule, as well as the buildings users' occupation and activity are simulated by means of the Type 56. TRNSYS is also used to accurately model all of the plant components. The work also includes comprehensive energy, environmental and economic analyses to maximize the plants profitability, evaluated by considering both operating and capital costs. Sensitivity analyses aiming at establishing the optimal values of the most important design parameters are also performed. The developed plants achieve important savings in terms of carbon dioxide emissions due to the use of renewable energy sources and the high efficiency of the included technologies. The best economic indexes are obtained for the layout using electricity-driven technologies, resulting in very profitable operation with a payback period of about 6.2 years.

1. Introduction

Renewable polygeneration systems are becoming increasingly attractive in the transition toward a zero-carbon society expected by 2050. Polygeneration plants play a key role in the energy-water nexus since the integration of different energy and water technologies in the same facility allows one to maximize the system efficiency. In particular, polygeneration systems represent a key solution for remote and

inaccessible communities (medium or small islands) providing space heating and cooling, electricity, and desalinated water in a single system. This combination allows one to optimize the use of energy cascades (heat and/or electricity) for freshwater production. For remote islands, characterized by a large availability of seawater, abundant renewable energy sources, and limited availability of conventional fossil fuels and fresh water, the concept of polygeneration is a very attractive option [1].

* Corresponding author.

E-mail addresses: francesco.calise@unina.it (F. Calise), francescoliberato.cappiello@unina.it (F.L. Cappiello), maria.vicidomini@unina.it (M. Vicidomini), fpetrako@ing.uc3m.es (F. Petrakopoulou-Robinson).

Nomenclature		η_{el}	electrical efficiency
<i>Subscripts and superscripts</i>			
A	area, (m^2)	<i>a</i>	Ambient
AF	annuity factor, (-)	AH	auxiliary heater
C	cost, (€)	<i>ap</i>	Aperture
c	specific Heat [$J/kg/K$]	back	back surface
CPVT	concentrating PhotoVoltaic Thermal solar collectors	cell	photovoltaic cell
C_{PVT}	concentration ratio	cool	Cooling
I_b	beam radiation [W/m^2]	conc	Concentrator
I_{tot}	total radiation [W/m^2]	conv	Convective
h_c	convective heat transfer coefficient [$W/m^2/K$]	dhw	domestic hot water
h_f	fluid specific Enthalpy [J/kg]	el	Electric
\dot{m}_f	fluid mass flow rate [kg/s]	<i>f</i>	Fluid
\dot{P}	electric power, (kW)	heat	Heating
r	area specific thermal resistance [m^2K/W]	<i>in</i>	Inlet
T	temperature, ($^\circ C$ or K)	ins	Insulation
v	voltage, (V)	MED	multi effect distillation
V	volume, (m^3)	mp	max power
E	energy, (kWh)	N	Number
I	current, (A)	net	Net
J	capital cost, (€)	oc	open-circuit
j	specific cost-price, ($€/m^3$)	out	Outlet
M	maintenance, (€/year)	ref	reference conditions
NOCT	nominal operating cell temp, ($^\circ C$)	rec	Receiver
PI	profit index, (-)	RO	reverse osmosis
<i>Greek symbols</i>		sky	referred to sky
α	Absorptance	sub	Substrate
ε_R	Emittance	th	Thermal
ε	heat transfer effectiveness	TK	Tank
Δ	Difference	<i>th</i>	Thermal
ρ_{PVT}	PVT Reflectance	<i>top</i>	top surface
σ	Stephan-Boltzmann constant	u	Unit
η_{th}	thermal efficiency		

Solar energy is considered one of the most promising renewable energy sources [2], available almost all over the world with different intensities. It can be used as an energy input of polygeneration plants, including solar thermal collectors and photovoltaic (PV) panels. In fact, in solar-powered polygeneration plants, different solar technologies can be included for the direct conversion of the solar irradiation into heat available at different temperatures, according to the adopted solar thermal technology. For example, in case of low or medium temperature levels, the produced heat is employed in solar heating and cooling (SHC) systems and/or domestic hot water (DHW) applications [3]. SHC technology, converting the solar irradiation into space heating and cooling, is particularly interesting in summer, when the cooling energy demand is often simultaneous to the availability of solar radiation. PV panels are used for the direct electric energy production and they are commonly coupled with electric vapour compression chillers. Hybrid PV-Thermal (PVT) collectors [4,5] for combined heat and power production are nowadays one of the most interesting applications for the simultaneous production of useful thermal and electrical energy. In case of low-temperature heat (residential applications), thermal energy is usually exploited for domestic hot water (DHW) preparation or space heating purposes. In addition, due to the lower PVT operating temperature - with respect to PV panels - the power production occurs at higher electrical efficiencies. In solar trigeneration plants, PVT solar collectors can be combined with single-stage Lithium Bromide / Water (LiBr/H₂O) absorption chillers for the production of cooling, heating, DHW and electric energy [6].

For freshwater production, several desalination techniques are available: Multi Stage Flash (MSF), Multi Effect Distillation (MED),

Thermal and/or Mechanical Vapor Compression (TVC, MVC), Reverse Osmosis, (RO), and Electrodialysis (ED). Some of these technologies (MSF, MED, TVC) use thermal energy to convert seawater into freshwater. Other technologies (RO, ED) are driven by electricity. Therefore, desalination units can also be easily coupled to a plurality of renewable energy sources and/or energy cascades. In MED systems, seawater is desalinated by a series of heating and evaporation processes, until freshwater is produced [7]. This technique is quite flexible in both operating temperature and capacity range (also higher than 20.000 m³/day of freshwater). This makes this technology especially attractive for small-medium scale communities in remote zones such as islands. RO is an electrically-driven desalination technology. In RO, fresh water, under high pressure, passes through semi-permeable membranes, leaving behind the high-concentrated brine solution. More than 50% of the worldwide installed desalination plants are based on RO technology due to its simplicity and relatively low energy cost and energy consumption [8]. As mentioned before, desalination technologies are also often coupled with renewable energy sources and a number of theoretical and experimental studies are available in this field. However, there is no consensus regarding the most profitable desalination technology, since this selection also depends on a number of additional external parameters. Therefore, one of the aims of this work is the comparative analysis of different desalination technologies, depending on different system layout configurations. In particular, in this work, the most promising thermal and electrical desalination technologies (MED and RO, respectively) are analysed considering different poly-generation plants. Here, when the MED process is included into the plant, solar thermal collectors are implemented, while electricity

produced by PV or PVT panels is used to drive the RO process, in other system configurations.

Several technologies can be combined in polygeneration systems producing electricity, heating, DHW and freshwater [9]. Buonomano et al. [10] investigated Concentrating Photovoltaic Thermal (CPVT) collectors coupled with a gas turbine, Absorption Chillers (ACHs) and suitable thermal storage tanks to supply energy to a hospital. Acceptable pay-back periods (from 4 to 6 years) are obtained in case of feed-in tariff scenarios on the produced thermal and electric energy. Linear Fresnel reflector (LFR) and evacuated tube solar collectors (ETC) coupled with a MED system, an auxiliary biomass-fired heater and absorption technology are evaluated in reference [3]. In this case a single-effect LiBr-H₂O Absorption Chiller (ACH) is considered when ETCs are included, whereas a double-effect ACH is included if LFR collectors are used. For the analyzed case study of Naples (South of Italy) characterized by a medium beam-to-total radiation ratio value, ETCs resulted more profitable than LFRs, achieving SPB periods of about 4–5 years, in the case of feed-in tariff incentives. The economic and energy feasibility of a solar-assisted system in different Italian weather zones for school buildings was assessed in reference [11]. Here, a single-stage LiBr/H₂O ACH, ETCs and a conventional electric-driven reversible heat pump (HP) are hybridized in a polygeneration plant for heating, cooling and DHW production. Such a system allows one to obtain significant energy savings: 52, 4%, 61.4% and 63.2% for Milan, Trapani and Naples, respectively. As it happens for the great majority of renewable energy systems, the feasibility of the plant is positive only in case of public funding policies with Simple Pay Back (SPBs) ranging from 12 to 16 years for Naples and Milan, respectively. Low temperature PVT collectors can be suitably coupled with solar-assisted heat pumps [12] and adsorption chillers [13] in novel solar-based polygeneration systems. In particular, during the winter, thermal energy of the PVT collectors mainly supplies the heat pump evaporator, whereas in summer, it supplies the adsorption chiller (usually activated for lower hot fluid temperatures) providing energy for space cooling. Such a system is not profitable without public incentive (simple payback period, SPB, higher than 16 years) and becomes profitable with capital investment subsidy of 50%. A solar heating and cooling (SHC) system is coupled with concentrating photovoltaic/thermal (CPVT) collectors (parabolic trough collectors, PTC, with triple-junction solar PV cells) and an electrolyzer [14]. The electrolyzer is driven with electricity produced by the CPVT and generates hydrogen, used in the fuel cell (FC), and oxygen, which is sold. Another hybrid polygeneration layout, combining a polymer electrolyte membrane fuel cells (PEMFC), a PEM electrolyzer, a lead acid battery, a wind turbine, monocrystalline PV panels, a metal hydride tank, a RO desalination unit, using energy recovery, and a hydrogen (H₂) vehicle is presented in reference [15]. Results show a technically feasible polygeneration microgrid adapted to small islands financially profitable with a probability of 90% for the present and 100% in the medium term.

In literature, special attention is paid to the issue of the stability of the supply in island systems, which are strongly dependent on renewable energy sources (RESs). The challenge is their energy self-sufficiency taking into account the limited availability of local fossil sources. In fact, islands are featured by a large availability of seawater, abundant RESs, and limited availability of conventional fossil fuels and fresh water. The goal of many works is the development of future 100% RES islands. For example, this issue is addressed in the work reported in reference [1], where a hybrid solar and geothermal polygeneration system combining CPVT collectors, a single-stage LiBr/H₂O ACH and a MED unit was studied. The plant supplies electric, thermal and cooling energy, DHW and a certain amount of desalinated water able to cover the whole request of the Pantelleria Island, assumed as case study. In particular, solar thermal energy, at a maximum temperature of about 100 °C, in combination with the thermal energy produced by low-enthalpy (about 80 °C) geothermal wells, is used to supply the MED system. Geothermal energy is also used to produce DHW at 45 °C. The

performance predicted through dynamic simulations, supported by appropriate economic models, was excellent. This work is particularly interesting because it presents a comprehensive assessment on combination of different kinds of technologies (SHC, CPVT, geothermal wells and MED). Several additional islands in the Italian Mediterranean Sea, Ischia and Aeolian Islands, showing a similar potential in terms of availability of geothermal and solar energy, are also investigated. For all the investigated locations, a parametric analysis aiming at evaluating the variation of Profit Index as a function of the ratio of DHW produced by the system and demanded by the user is performed. It resulted that Profit Index dramatically decreases in case of scarce DHW demand. Other studies concerning the dynamic simulation of a novel hybrid solar and geothermal polygeneration system capable to produce electric energy, fresh water and space heating and cooling, for the Pantelleria Island was presented and discussed in references [16] and [16]. Here, with respect to the previous layout, an Organic Rankine Cycle (ORC) supplied by geothermal and solar energy is considered. In particular, in reference [1], a low-temperature geothermal well (85 °C) is used, mainly for the desalination process, whereas in references [16] and [16] a medium-enthalpy geothermal source (160 °C) is considered. In addition, in this work, CPVT collectors are replaced by Parabolic Trough Collectors field coupled to a thermal storage tank. From the energy analysis it resulted that the solar energy input is much lower than the geothermal one, as shown by the low value found for the solar fraction, 9.60%. During the year the MED unit is able to produce fresh water, equal to 54% of the total seawater flowrate. Using an accurate energy, economic, exergy and exergoeconomic analysis of the system, it was found out that the global exergy efficiency varies from 40% to 50% during the thermal mode and from 16% to 20% during the cooling one; besides, the exergoeconomic costs of electricity, cooling water, chilled water and desalinated water resulted very interesting, respectively in the ranges 0.1475–0.1722 €/kWh, 0.01612–0.01702 €/kWhex, 0.1863–0.1888 €/kWhex and 0.5695–0.6023 €/kWhex. The previous works [16] are developed by considering that all the useful products are consumed by the user. Instead, in a further study [17], based almost on the same plant configuration, the system is supposed to be connected to a district electric, heating and cooling network. In this case, system energy production must match the real time-dependent demands of electricity and space heating and cooling of typical buildings of Pantelleria Island (assumed as a case study). The system achieved a SPB equal to 8.50, with a potential primary source saving of 3039 t and a potential CO₂ avoided emission of 9451 t. The system can cover the energy demands of 800 examined buildings. Moreover, the plant produces 1006 10³ m³ of desalinated water and it is capable to cover the fresh water global demand. Average ORC efficiency amounts to 15.30%. The system is mainly powered by geothermal energy, in fact, the average solar fraction of the system is only 14.6%.

A 100% RESs system for Astypalaia island in Greek based on wind turbines, concentrating solar power (CSP) plant and desalination units is proposed in the work of Wang et al. [18]. The flexible scheduling of CSP plants is used to complement to the wind power generation, and the thermal storage system reduces the battery energy storage configuration for islands. By appropriately planning the capacity of MED and RO units, these can meet the freshwater demand by effectively utilizing surplus electric power and low-grade waste heat from the CSP plant. Main findings of the works regard the improved thermal energy utilization efficiency of the system and the cogeneration of water and electricity, when the latent heat of the low-grade waste heat from the CSP plant, although the coupling of the CSP plants and MED units reduce the power generation efficiency. The proposed system is more flexible in scheduling, and it reduces the investment for energy storage systems. Karavas et al. [19] presented a techno-economic study of freshwater production by PV panels and RO technology in the Aegean islands. The scenario of the proposed technologies is supposed to replace the current water supply systems of these islands, based on the water ships. The operating modes of the RO plant at nominal or variable

load are also considered. Simulations of five different scenarios are performed with and without electrical or water storages. The aim is to optimize the unit cost of water obtaining the optimal values of the water storage tank volume and PV and battery system capacity. The better solution is obtained for the scenario including PV panels coupled with water tank, batteries and variable load operation of RO desalination units, with a cost of 3.75 €/m^3 , which is obviously much lower than the cost of transported water, equal to 12.77 €/m^3 . A further study regarding a solar thermal polygeneration system integrating membrane distillation was also investigated by Mohan et al. for United Arab Emirates locations [20]. Here, with respect to the previous solar poly-generation system, the solar energy is directly provided to the desalination unit. A 35.2 kW single stage LiBr/H₂O ACH is also included in the system in order to meet the cooling load in a portacabins building, modelled in TRNBUILD and located in Rakric. The whole system, designed for also producing DHW as coproduct, is modelled in TRNSYS environment and validated by the experimental data achieved from on-site testing of polygeneration system. In this study, three different solar technologies were compared: flat plate, evacuated tube and compound parabolic collectors. Dynamic simulations, developed in TRNSYS

environment, showed that the best pay-back value, equal to 6.75 years, was achieved in case of evacuated tube collectors having gross area of 216 m^2 . The best performance in terms of daily production of membrane distillation and DHW production 92.8 kg/day and 301.67 kg/day, respectively.

In the framework of polygeneration systems for Islands, the conversion of fossil fuels or of renewable energy source, aiming at reducing the environmental pollution, mainly in the transportation sector, has recently attracted a significant interest. For example, Pfeifer et al. [21] analyse the use of zero emission ferry lines (hydrogen and fully electricity fuelled ferries), for the interconnection and connection to the mainland for different Croatian islands (Mediterranean Sea). The availability of the solar and wind energy sources of the Croatian island of Korčula exploited to supply both road transport but also ferry lines is investigated in reference [22]. In particular, smart charging vehicles and ferries are connected to the grid and allow charging and discharging of the batteries. The development of 100% RES islands is addressed for Croatian Islands of Vis, Korcula, Lastovo and Mljet in the work proposed in reference [23]. The interconnections of a group of islands integrating the production from locally available RES is

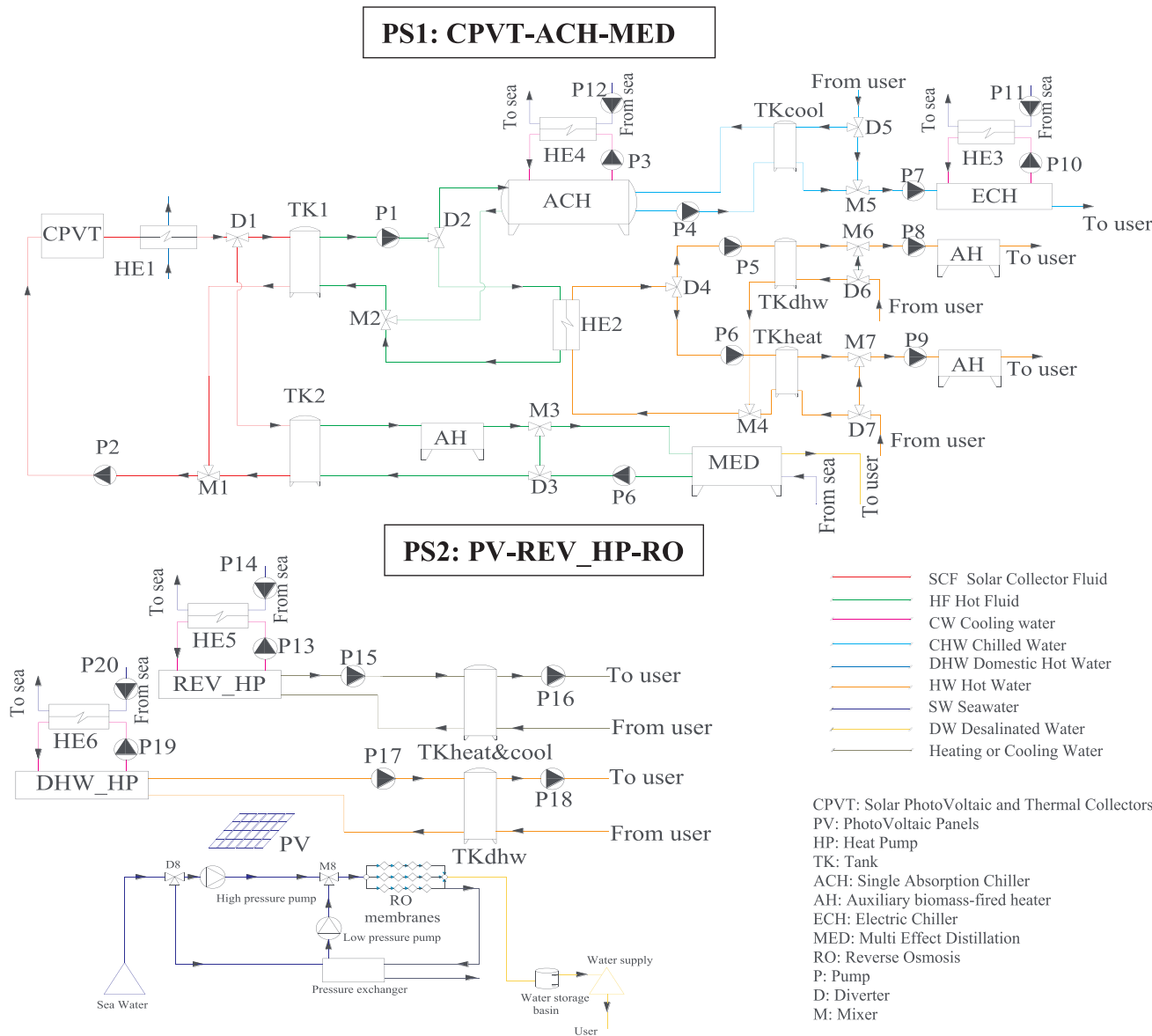


Fig. 1. System layouts.

proposed. In particular, for the year 2035 the vehicle-to-grid concept is implemented to use electric vehicles as potential storage systems for the variable energy production. The issue of the Islands interconnection to achieve 100% RESs is addressed also in the Azorre archipelago, the Pico and Faial Islands, by Alves et al. [24]. The mismatch between demand and supply and the stability issue are also discussed in this paper.

1.1. Novelty and aim of study

The above reported literature review clearly shows that it is important to achieve 100% renewable energy islands, implementing different energy actions to guarantee the self-sufficiency energy supply and network stability. The literature review also shows that virtually infinite polygeneration layouts can be conceived, due to the large number of combinations of the available renewable sources, energy conversion and desalination technologies. However, the above reported literature review shows that most of the published studies about this topic only focus on a single specific polygeneration plant. There is no consensus regarding the most profitable system layout, nor regarding the integration of the different available renewable and desalination technologies. No comprehensive study is available in literature comparing electrically and thermally driven desalination technologies on combination with renewables in polygeneration systems serving islands.

In fact, to the best of the authors' knowledge, none of the papers available in literature compare different polygeneration plants producing water and energy, simultaneously considering energy and economic aspects, comparing different renewable and desalination technologies. This work aims to address this gap, presenting a comparative study of different polygeneration layouts including different solar and desalination technologies. In particular, in the present work both PV and CPVT technologies are considered in different combinations with other devices. In particular, solar subsystems were coupled with different thermal energy activated technologies (TATs), such as single ACH, MED desalination units or with electric energy activated technologies (EATs), such as electric vapor compression chillers and RO desalination units. The present study considers different combinations of the above-mentioned technologies in order to detect the best combination from both energy and economic points of view. Note that one of the layouts considered in this work is based on the one reported in reference [25]. However, with respect to the cited previous study, the present work includes further improvements. In fact, in reference [25] it is assumed that all the produced energy and water is consumed by the user, independently of the demands of specific districts. This simplifying assumption allowed one to significantly simplify the calculations since the estimations of user energy and water time-dependent demands was not necessary. This simplifying assumption is removed in the present work, where the hot and cold water loops are hydraulically connected with the selected district systems where heat, cool, electricity and water time-dependent demands are carefully estimated. To this scope, detailed building clustering is implemented. Then, advanced building dynamic simulations are performed in order to evaluate district energy and water demand in combination with measured data. In particular, for each time step of the simulation, the heat, cool, electricity and water production are compared with the related user demands. Finally, the results of this study can be used in a more general manner to design polygeneration systems, producing space heating and cooling, DHW and freshwater for small Mediterranean Islands.

2. System layout

Two layouts of the investigated plants are shown in Fig. 1. The first layout "CPVT-ACH-MED" is mainly based on the layout reported in reference [25], combining SHC, CPVT collectors, a biomass auxiliary heater, a LiBr-H₂O single-effect ACH, and a MED unit. The same control strategies reported in reference [25] are implemented using suitable

controllers (feedback, proportional and on/off) and schedulers (daily and seasonal). Note that reference [25] did not consider any specific user demand since the authors assumed that all the produced energy and water could be consumed by the user. This simplification is not considered in the present paper and the hot- and cold-water loops are hydraulically connected with the respective systems of the buildings included in the district. Therefore, in the presented study the production of energy and water must be compared with the time-dependent user demand. As a consequence, a detailed control strategy is also implemented in order to manage the system operation and to match the heating, cooling and DHW demand of the district users. For this purpose, further auxiliary devices are included in the SHC network in order to cover the district demand when the solar radiation is low and/or user demand is high. This additional equipment includes an electric chiller (ECH) for space cooling and wood-chip auxiliary heaters (AH) for DHW and space heating. The set point temperature of the AH for space heating $T_{setAH,heat}$ is 55 °C and the set point temperature of the AH for DHW $T_{setAH,DHW}$ is 45 °C. During winter, after the pump P1, the diverter D2 diverts the hot water to the district network for space heating and DHW, i.e. to the heat exchanger HE2; during summer the diverter D2 diverts the hot water to the set district network for space cooling. The water of the secondary loop is heated in the heat exchanger HE2 and it is further divided with the diverter D4 to the DHW and space heating networks by means of the pumps P5 and P6, respectively. Two hot water stratified storage tanks, TKdhw and TKheat, are expected to manage the fluctuations of the district demand. Pumps P8 and P9 collect the hot water from the top of the tank to supply the users. A by-pass circuit consisted of diverters and mixers in both the DHW and heating networks is also included. Therefore, when the tank top temperature is lower than $T_{setAH,heat}$, the diverter D7 (or D6) directs the return water from the user to the AH, which heats it up the selected set point temperature. When the tank top temperature is higher than $T_{setAH,heat}$, the diverter D7 directs a part of the return cold water from the user to the M7 to obtain the hot water at the selected set point. This occurs until the tank top temperature decreases to $T_{setAH,heat}$. The bottom water of both tanks on the secondary circuit returns to the heat exchanger HE2 with the mixer M4 to get reheated and continue the loop. When no heating is required, D2 diverts a part of the hot water to the HE2 to cover the demand for DHW. Therefore, D4 closes the exit in the direction of the tank TKheat. During the cooling season, a certain amount of the hot water supplies the ACH, which produces chilled water at 6.5 °C stored into a further stratified storage tank TKcool. To cover the cooling demand, the chilled water is pumped by pump P7 from the bottom side of the tank to the user. The electric chiller is switched on when the bottom temperature of the tank is lower than 7 °C. In this case, a by-pass circuit is also included. In order to cool ACH and ECH, two heat exchangers supplied with seawater at a constant temperature of 25 °C, (reasonable value for the Mediterranean Sea) are used.

The second layout "PV-REV_HP-RO" includes PV panels coupled with a RO unit, which produces freshwater, and two different electric heat pumps for the separated production of space heating, cooling and DHW. Therefore, two water-to-water reversible heat pumps (REV_HP), operating in parallel, are included to match the space heating and cooling energy demand. During the winter operation, the district supply hot water temperature is set at 45 °C, appropriate value to supply the fan coil units. To guarantee the correct operation of the heat pumps and avoid continuous switching on/off, a suitable controller and a stratified storage tank TKheat&cool are included. The controller reads the top temperature of the tank TKheat&cool and when the tank top temperature is lower than 44 °C, heat pumps are switched on. This circumstance occurs until the tank top temperature is higher than 45 °C. During summer operation, it is assumed that the temperature of the chilled water on the fan coil units ranges between 13 and 15 °C. This occurs by a further suitable controller reading the bottom temperature values of the tank TKheat&cool and managing the activation of the heat pumps. In particular, heat pumps work when the bottom temperature is greater

than 13 °C and they are switched off when the temperature reaches 11 °C. For DHW production, two water-to-water heat pumps (DHW_HP), operating in parallel, are designed to supply DHW at 45 °C to the users. The electricity produced by PV panels is used to supply first the RO unit and then the heat pumps. A variable level water storage basin, aiming at storing the produced freshwater, is also included. In particular, if the production of the RO unit is higher than the district water demand, the surplus is supplied to the basin, which stores the produced freshwater. Conversely, when the solar radiation availability is scarce and/or if the district water demand is higher than the RO production, the stored desalinated water is supplied to the user. In this way, the dependency of the island on the freshwater supplied by ships is reduced. Details regarding the layout and some special control strategies adopted to allow the proper operation of the RO unit are reported in reference [8]. Note that such a plant is not equipped with water or electric storage systems. Therefore, when the PV panels production is scarce, with respect to the energy demand of RO unit and heat pumps, the necessary electricity is supplied from the grid. Conversely, the electric excess is delivered to the grid.

3. System model

All the components included in the investigated plants are modelled by adopting models provided in the dynamic simulation tool TRNSYS 17 [26]. This is a well-known software in the academic community and is successfully used to carry out dynamic analyses of several types of solar systems [27]. Note that the studied layouts do not exist yet, so, a validation against a real system is not possible. Nevertheless, the models of TRNSYS are based on unsteady algorithms and they are validated using experimental data or based on manufacturers' data. The achieved results are, therefore, considered highly reliable and it can be assumed that the plants are validated. For the sake of brevity, the complete models of the incorporated components (pumps, diverters, mixers, diverters, heat exchangers, auxiliary heaters, etc.) are not reported here, since they were presented in a recent works developed by some of the authors [8]. In the following, some brief details about these components is provided.

- Type 94, modelling the performance of photovoltaic panels, by considering the electric performance of the poly-crystalline/crystalline silicon cells. The so-called “four parameters” model, described in reference [26] is used. Type 94 calculates the four parameters values from manufacturers' data in order to generate an IV curve at each time step.
- Type 4, simulating the energy storage tanks providing thermal energy for space heating, DHW, cooling, and the energy for seawater desalination. They consist of fluid-filled sensible vertically stratified tank, modelled by dividing the tank in n fully-mixed nodes with equal volumes [26];
- Type 107, using a map catalogue approach to simulate the performance of the LiBr-H₂O single effect absorption chiller at any time step of the simulation [26];
- Type 927, modeling a single-stage water-to-water reversible heat pump. This model is based on user-supplied catalog data file containing the normalized capacity and power draw, based on the entering load and source temperatures and the normalized source and load flowrates [26];
- Type 56, simulating the dynamic energy performance of the district buildings in terms of heating and cooling loads. In particular, Type 56 takes into account the 3D geometry (by means the Google SketchUp TRNSYS3d plug-in [28]), envelope thermophysical properties, and indoor (i.e. lighting, machineries heat gains schedule as well as the buildings users' occupation and activity) and environmental conditions of the buildings (i.e. solar radiation, ambient temperature, humidity) etc. For further details see reference [2].

The user-developed models by other tools and then included into the TRNSYS environment by the authors are:

- the heat exchangers HE1 and a flat-fin compact heat exchanger for DHW production are developed using a modified version of the well-known ϵ -NTU method [34]; details are reported in reference [29];
- the MED model is reported in reference [25]. The model consists of a stationary model based on mass and energy balances and heat transfer equations applied to i) the first effect, supplied by solar energy; ii) the second to the last effect, and iii) the condenser;
- the triple-junction concentrating PVT collector model, based on zero-dimensional energy balances, reported in reference [30];
- the RO unit model based on the Solution-Diffusion model [31–33], that is one of the most widely accepted description for the RO process. The detailed model of the RO unit (in-house developed by a zero-dimensional approach) and its validation are reported in reference [8];
- the energy and economic model developed to evaluate the energy and economic performance of the plants.

In the following the energy, economic and environmental model, as well as the CPVT and RO models are described.

3.1. CPVT collector model

This collector consists of a parabolic trough concentrator and a linear triangular receiver, located at the focus of the parabola, with the lower surface equipped with a triple-junction InGaP/InGaAs/Ge, whereas the upper surface is equipped with an absorber surface. By energy balances developed in EES (Engineering Equation Solver), the temperatures and energy flows of the main components of the collectors are calculated. Therefore, the overall energy balance on a control volume including the entire receiver (from PVT to the insulation) is:

$$\begin{aligned} A_{rec} I_b C_{PVT} \eta_{opt} + A_{top} I_{tot} \alpha_{top} &= \dot{m}_f (h_{out} - h_{in}) + C_{PVT} A_{rec} I_b \eta_{opt} \eta_{PV} \\ &+ A_{rec} I_b C_{PVT} \eta_{opt} \rho_{PVT} + A_{top} \epsilon_{R,top} \sigma (T_{top}^4 - T_{sky}^4) \\ &+ A_{PVT} \sigma \epsilon_{R,PVT} (T_{PVT}^4 - T_{conc}^4) \\ &+ A_{PVT} h_{c,PVT} (T_{PVT} - T_a) + A_{top} h_{c,top} (T_{top} - T_a) \end{aligned} \quad (1)$$

A second energy balance considers the control volume that includes the metallic substrate and the fluid channel, assumed as a heat exchanger, and it is:

$$\dot{m}_f (h_{out} - h_{in}) = \dot{m}_f c_f (T_{sub} - T_{in}) \quad (2)$$

in which T_{sub} is the temperature of the metallic substrate.

For the given boundary conditions (beam and total radiations and relative angle of incidence, inlet temperature and mass flow rate, environment and sky temperature, ambient pressure and wind velocity), the unknown variables are five, namely: PVT temperature, substrate temperature, fluid outlet temperature, temperature of top receiver surface (facing the sky), and temperature of the concentrator. Therefore, three more – a total of five – equations must be considered. The third required equation is derived from an energy balance on a control volume including the PVT layer and the metallic substrate.

$$A_{rec} \frac{T_{PVT} - T_{sub}}{r_{PVT-sub}} = \dot{m}_f (h_{out} - h_{in}) + A_{top} \frac{T_{sub} - T_{top}}{h_{top}} \quad (3)$$

The fourth energy balance can be considered with respect to the control volume that includes the top side of the substrate and the top surface of the triangular receiver:

$$\begin{aligned} A_{top} \frac{T_{sub} - T_{top}}{r_{top}} + A_{top} I_{top} &= A_{top} I_{top} \rho_{top} + A_{top} \epsilon_{R,top} \sigma (T_{top}^4 - T_{sky}^4) + A_{top} h_{c,top} (T_{top} - T_a) \end{aligned} \quad (4)$$

Finally, the last energy balance considers the control volume that

includes only the parabolic concentrator:

$$\begin{aligned} A_{PVT}\sigma\varepsilon_{PVT}(T_{PVT}^4 - T_{conc}^4) + I_{tot}A_{conc}\alpha_{conc} = A_{conc}\sigma\varepsilon_{conc,back}(T_{conc}^4 - T_{sky}^4) + \\ A_{conc}h_{c,conc,front}(T_{conc} - T_a) + A_{conc}h_{c,conc,back}(T_{conc} - T_a) \end{aligned} \quad (5)$$

Due to the radiative terms, the system of equations is not linear and it must be solved iteratively. This CPVT model is stationary, but this assumption can be removed by adding capacitive terms in the balances, and consequently, converting the system into a differential equations system that can be solved using well-known techniques also included in the EES tool. It is possible to calculate thermal and electrical efficiencies using the following equations:

$$\eta_{CPVT,th} = \frac{\dot{m}_f(h_{out} - h_{in})}{A_{ap}I_b} \quad (6)$$

$$\eta_{CPVT,el} = \frac{C_{PVT}A_{PVT}I_b\eta_{opt}\eta_{PV}}{A_{ap}I_b} \quad (7)$$

3.2. District heating and cooling networks

District heating and cooling networks bring several short- and long-term benefits for communities. In this paper, energy generation from the proposed renewable energy systems is distributed to communities, offering the opportunity for higher penetration of renewable energy to community members and remote areas that may otherwise not permit viable on-site renewable energy use. In addition, the use of renewable-based energy for heating and cooling purposes reduces the use of fossil fuels, reducing the overall environmental impact of energy conversion.

To evaluate some technical requirements of the heating and cooling systems assumed in this study, basic simplified indicators and costs of the piping system have been calculated. The pipe length required per building has been calculated using the equation:

$$L_{spec} = 1207.36\rho_{building}^{-0.5894} \quad (8)$$

where $\rho_{building}$ is the building density, i.e., the buildings per km² [34]. A smaller number of buildings needs a smaller piping network, reducing the cost of the system. The total annual energy of the systems in this study include the heating and cooling or the domestic hot water supply to the communities. The cost of the distribution network is calculated as

$$CAPEX = (C_1 + C_2 d_a)L_p \quad (9)$$

with $L_p = 0.02A_{DH} + 0.4A_{DHW}^{0.5}$, d_a is the diameter of the pipes and C_1 and C_2 the construction cost constant and the construction cost coefficient. The diameter of the pipes can be calculated using the logarithmic equation presented by Persson and Werner [35]. However, the two regions investigated in this study are rural areas with low population density that include a high number of secondary or vacation residences with relatively low annual energy demand. The linear density of the case studies is, thus, found to be smaller than 1 MWh/m and the average pipe diameter of the networks has been assumed to be 35 mm [34]

3.3. RO model

The model of the RO unit has been developed in-house using a zero-dimensional approach and is based on a pressure driven membrane process [36], equipped by a Pressure Exchanger (PX). PX is a device that transfers the hydraulic energy of the pressurized brine directly to the feed seawater without an intermediate conversion to mechanical energy, resulting in high efficiencies. The model, written in MATLAB, is subsequently linked to TRNSYS. The input parameters to the RO simulation model are: i) seawater temperature ii) seawater concentration, iii) seawater feed flowrate to the RO membranes and iv) seawater feed pressure to the RO membranes. The in-house RO model is based on

the following equations:

$$\dot{W}_{p,i} = A_w \cdot A_{membranes} \cdot (\Delta P_{ri} - \Delta \Pi_i) \quad (10)$$

$$\dot{m}_{s,i} = B_s \cdot A_{membranes} \cdot (c_{f,i} - c_{p,i}) \quad (11)$$

where, $\dot{W}_{p,i}$ is the permeate water flowrate [m³/s], B_s is the salt permeability coefficient [m/s], ΔP_{ri} is the pressure of the seawater feed flowrate on the inlet of the RO module [Pa], A_w is the water permeability coefficient [m³/(Pa m² s)], $\Delta \Pi_i$ is the osmotic pressure of the seawater [Pa], $c_{f,i}$ and $c_{p,i}$ are the feed seawater and the permeate water salt concentration [mol/m³], and $\dot{m}_{s,i}$ is the mass flowrate of salt that is able to pass across the membrane [kg/s].

$\Delta \Pi_i$ is evaluated step by step according to the Van't Hoff's law:

$$\Delta \Pi_i = k_s R T_i (c_{f,i} - c_{p,i}) \quad (12)$$

where, T_i is the absolute temperature of the seawater (obtained by adopting the hourly data measured by the ISPRA institute [37]), R is the universal gas constant [J K⁻¹ mol⁻¹], and k_s is the number of ions of the salt molecule.

A_w and B_s show the performance of the RO membrane/module and they depend on T_i and on the type of the selected membrane. To consider the effect of the membrane compaction due the high pressure on the membrane, the value of the A_w is modified step by step as a function of the value of the pressure on the membrane, by considering this empirical correlation [33,38]:

$$\frac{R_{membranes,i}}{R_{membranes,0}} = \exp\left(1 - \frac{\Delta P_{r0}}{\Delta P_{ri}}\right) \quad (13)$$

where, $R_{membranes}$ is equal to $1/A_w$ and it represents the hydraulic resistance of the membranes.

Further details, concerning the equations implemented for the evaluation of the RO module performance, in terms of Rejection Rej (i.e., the capability of the RO module to reject the salt, and to achieve drinkable water with a lower salinity), Recovery $Recov$ (the amount of drinkable water that is produced thought the RO module with respect to the amount of feed seawater), and PX efficiency, are provided in reference [8].

3.4. Energy, economic and environmental model

The proposed plants are analyzed from an energy, economic and environmental point of view by a suitable model calculating the primary energy saving (PES), the simple payback period (SPB), the profit index (PI), and the avoided carbon dioxide (CO₂) emissions (ΔCO_2). In particular, indexes are evaluated by comparing the proposed systems (PS) with a reference system (RS). In the RS?? the thermal energy demand of the district buildings for the space heating and DHW is provided by traditional boilers ($\eta_{BS,RS} = 0.80$) and space cooling is supplied by electrically-driven air-to-air heat pumps ($COP_{CH,RS} = 3$). Regarding the electric energy demand, it is considered that the local grid, based on diesel engine power plants (with an electric efficiency $\eta_{RS,el}$ assumed equal to 0.35), is the main source to cover the demand of the district (note that it is common for remote islands to not be linked to the national electric grid). The fresh drinkable water demand is provided by water-tankships.

PES is calculated as follows:

$$PES = \sum_i \left(\frac{E_{th,heat,RS} + E_{th,DHW,RS}}{\eta_{AH,RS}} + \frac{E_{th,cool,RS}}{COP_{CH,RS}\eta_{RS,el}} + \frac{E_{el,RS}}{\eta_{RS,el}} \right. \\ \left. - \frac{E_{el,fromGRID,PS}}{\eta_{RS,el}} + \frac{E_{el,toGRID,PS}}{\eta_{RS,el}} - \frac{E_{th,AH,PS}}{\eta_{AH,PS}} \right)_i \quad (14)$$

where, $E_{th,heat,RS}$ and $E_{th,DHW,RS}$ are the thermal energy demand for space heating and DHW of the district in RS, respectively; $E_{th,cool,RS}$ is the thermal energy demand for space cooling in RS; $E_{el,RS}$ is the electric

energy demand of the district in RS; $E_{el,toGRID,PS}$ and $E_{el,fromGRID,PS}$ are the electric energy delivered/withdrawn to/from the local grid in PS; the index i is related to the i -th time step of the simulation.

The model includes the evaluation of the total capital cost (J_{tot}) for each proposed plant, according to the summary reported in [Table 6](#). The total capital cost (J_{tot}) also includes the cost of the piping network as discussed in the previous subsection. The economic savings ΔC are evaluated by comparing the operating costs of the reference and proposed systems:

$$\Delta C = \sum_i \left[\left(\frac{E_{th,heat,RS} + E_{th,DHW,RS}}{LHV_{NG}\eta_{AH,RS}} \right) J_{NG} + \left(\frac{E_{th,cool,RS}}{COP_{CH,RS}} + E_{el,RS} \right) J_{el,fromGRID} \right. \\ \left. + M_{fw,demand} J_{water,ship} \right. \\ \left. - \left(M_{SolarField} + M_{DesalinationUnit} + E_{el,fromPS} J_{el,fromGRID} \right) \right. \\ \left. - E_{el,toGRID,PS} J_{el,toGRID} + \frac{E_{th,AH,PS}}{LHV_{biomass}\eta_{AH,PS}} J_{biomass} \right] \quad (15)$$

where, $J_{water,ship}$ is the specific cost of the water transported by ships; $J_{el,fromGRID}$ is the specific cost of the electric energy withdrawn from the grid; J_{NG} is the cost of natural gas; $J_{biomass}$ is the cost of the wood chip, and $LHV_{biomass}$ and LHV_{NG} are the low heating values of the wood chip and natural gas, respectively; $M_{SolarField}$ and $M_{DesalinationUnit}$ are the maintenance costs according to values reported in [Table 6](#). Note that the last term of Eqs. (1) and (2) is considered only in the proposed plant PS1, where the wood chip auxiliary heaters are used to cover the thermal energy demand for DHW, heating and desalination when the solar radiation is scarce or null.

The simple payback period, i.e., the ratio between the total capital cost J_{tot} of the proposed system and the yearly economic saving ΔC , and the profit index (PI) are calculated as follows:

$$SPB = \frac{J_{tot}}{\Delta C} \quad (16)$$

$$PI = \frac{\Delta C \cdot AF - J_{tot}}{J_{tot}} \quad (17)$$

where, AF is the Annuity Factor [years], depending on by the discount rate a [%] and the system time horizon TH [years].

The yearly avoided equivalent carbon dioxide emissions ΔCO_2 of the PS vs. the RS are also evaluated:

$$\Delta CO_2 = \sum_i \left(\frac{E_{th,heat,RS} + E_{th,DHW,RS}}{\eta_{B,RS}} \cdot F_{NG} + \left(\frac{E_{th,cool,RS}}{COP_{CH,RS}} + E_{el,RS} \right. \right. \\ \left. \left. - E_{el,fromGRID,PS} + E_{el,toGRID,PS} \right) \cdot F_{el} \right)_i \quad (18)$$

where, F_{el} is the CO_2 equivalent emission factor for electricity and F_{NG} is the CO_2 equivalent emission factor for natural gas,

4. Case studies

This paper proposes two polygeneration systems for supplying thermal and electric energy and fresh drinkable water to remote regions. The considered remote regions are Santa Maria di Salina and Favignana ([Fig. 2](#)).

The first part of this work deals with the characterization of the two remote regions, in order to estimate the thermal and electric energy demand, as well as the drinkable freshwater demand.

Santa Maria di Salina is a district of 8.75 km^2 of the Salina island, located in the archipelagos called Aeolian Islands (Tyrrhenian Sea, South Italy). This district consists of 852 buildings and 903 inhabitants. Since this district is an attractive touristic zone, an increase in the number of inhabitants is considered during the summer season. The electric- and thermal-energy demand of this district was estimated, modelling five kinds of representative buildings. In particular, building V1 is a single-family house of 93.24 m^2 , building V2 is a two-floor multi-family house, including two apartments of 93.24 m^2 ; Off is a two-floor office; H is a two-floor hotel, and Sch is a two-story school. SMS and F stand for the name of the area: Santa Maria di Salina and Favignana, respectively.

[Table 1](#) displays the geometrical features of the analyzed buildings, and [Fig. 3](#) shows the SketchUp modes.

Considering the year of construction of the district and the geographical location, it is assumed that the buildings of the island are poorly insulated (U equal to $1\text{--}1.4 \text{ W/m}^2 \text{ K}$), [Table 2](#). In particular, [Table 2](#) displays the features of the envelope and windows of each building. The number of district inhabitants increases during the summer seasons (May–September SS), reaching 1750 people, due to the increase of the touristic activity of the island.

In particular, it is assumed that only a limited number of houses are occupied during the winter season (October–April WS), whereas during the summer season all of the houses are occupied ([Table 3](#)). Moreover, the hotel occupation triplicates during the summer season. The offices are considered open during the whole year and the schools are closed from June to September, according to Italian regulation.

Favignana is an island of 19.3 km^2 in the Egadi archipelagos of the



Fig. 2. Case studies location.

Table 1

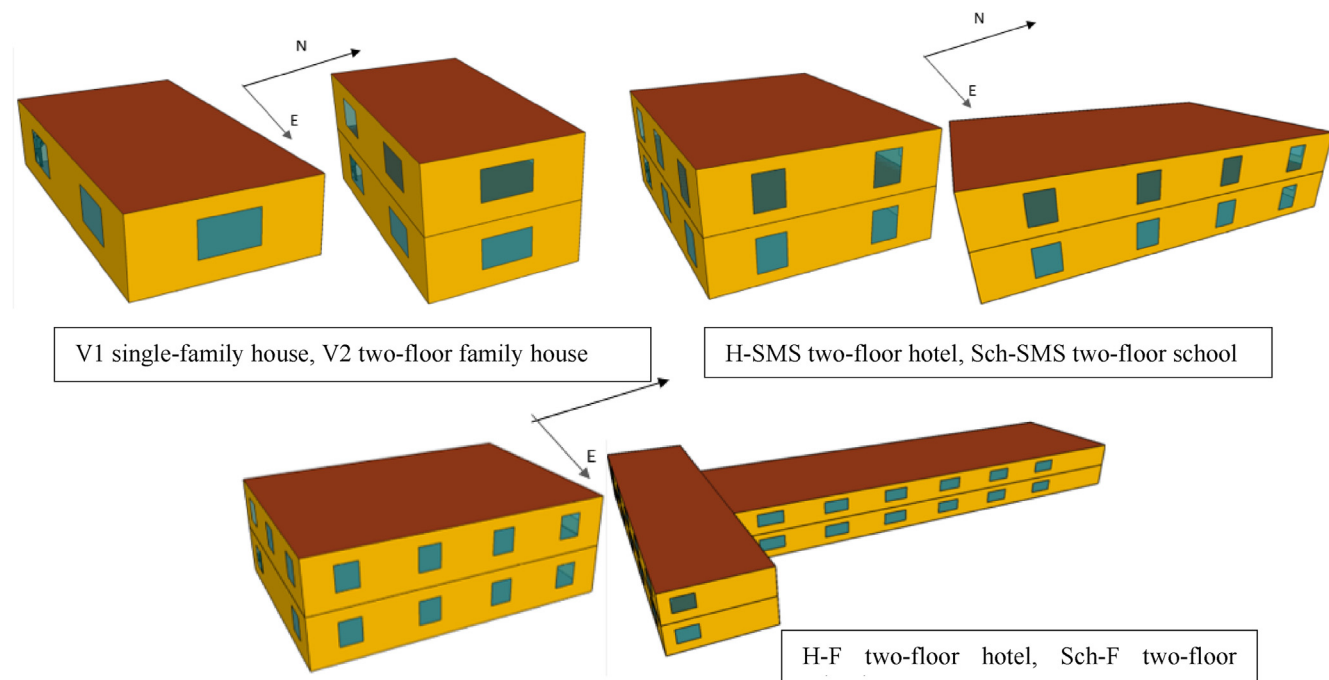
District simulation data: Santa Maria di Salina and Favignana.

Geometric features	Both districts		Santa Maria di Salina			Favignana		
	V1	V2	H-SMS	Sch-SMS	Off-SMS	H-F	Sch-F	Off-F
Height (m ²)	3	6	6	6	6	6	6	6
Volume (m ³)	280	559	1080	2655	1080	1209	5208	3750
Floor area (m ²)	93.24	93.24	180	442.5	180	201.45	868	625
Number of planes (-)	1	2	2	2	2	2	2	2
Number of apartments for floor (-)	1	2	—	—	—	—	—	—
Apartment area (m ²)	93.24	93.24	—	—	—	—	—	—
Glass area (m ²)	19.15	38.73	51.11	72.90	64.84	45.08	171.80	66.72
Heating and cooling season (Salina 669 HDD)	Heating: T _{set} = 20 °C 15th November-31 st March Cooling: T _{set} = 26 °C 1st May to 30th September							
Heating and cooling season (Favignana 686 HDD)	Heating: T _{set} = 20 °C 15th October-15th April Cooling: T _{set} = 26 °C 1st June to 15th September							
Thermal Energy demand	Figs. 4 and 5							
Air infiltration rate (vol/h)	0.6							
Average daily DHW demand (m ³ /day/person)	50							
DHW set point temperature (°C)	45							

Tyrrhenian Sea in South Italy. Favignana is modelled according to the same approach used for Santa Maria di Salina. In particular, the same representative types building are considered. Note that office, hotel and school buildings are featured by different geometrical features with respect to the ones considered in Salina (Table 1). Regarding the thermophysical proprieties of the buildings, no remarkable differences are assumed between the two locations. Since Favignana is a very attractive touristic place, a significant increase of the number of inhabitants is considered during the summer season, as for the case of Salina. In particular, the inhabitants of the island increase from 965 in winter to 2000 in summer. Table 3 displays the number of buildings occupied during the year. For the evaluation of the thermal energy demand of Favignana and Santa Maria di Salina, the heating and cooling seasons are assumed according to Italian regulation: Heating season from 15th November to 31st March and cooling season from 1st May to 30th September.

Proposed system PS1: CPVT-ACH-MED is referred to Favignana. This polygeneration plant includes a CPVT field that supplies a district heating and cooling network and MED technology that produces

drinkable freshwater. The MED system is driven with thermal energy from the CPVT collectors (Table 4). In particular, the district heating network directly uses the thermal energy provided by the CPVT collectors. Moreover, biomass heaters are installed as auxiliary systems, in order to match the thermal energy demand when the solar radiation is scarce or null. The district cooling network is supplied by an absorption chiller driven by thermal energy produced by the CPVT collectors. An auxiliary electric chiller is also installed for matching the cooling energy demand when the thermal energy produced by the CPVT collectors is not sufficient for the activation of the absorption chiller. Another district heating network provides the thermal energy for DHW preparation, using thermal energy from the CPVT field. A biomass auxiliary heater is installed for meeting the thermal energy demand for DHW preparation, when the thermal energy supplied by the CPVT is insufficient. Finally, the power demand, including the power delivered to electric components of the plant, electric chiller and district demand, is matched by power produced by the CPVT collectors. When the CPVT power production does not meet the district power demand, a suitable amount of power is withdrawn from the local grid. Conversely, the

**Fig. 3.** An example of the SketchUp 3D model.

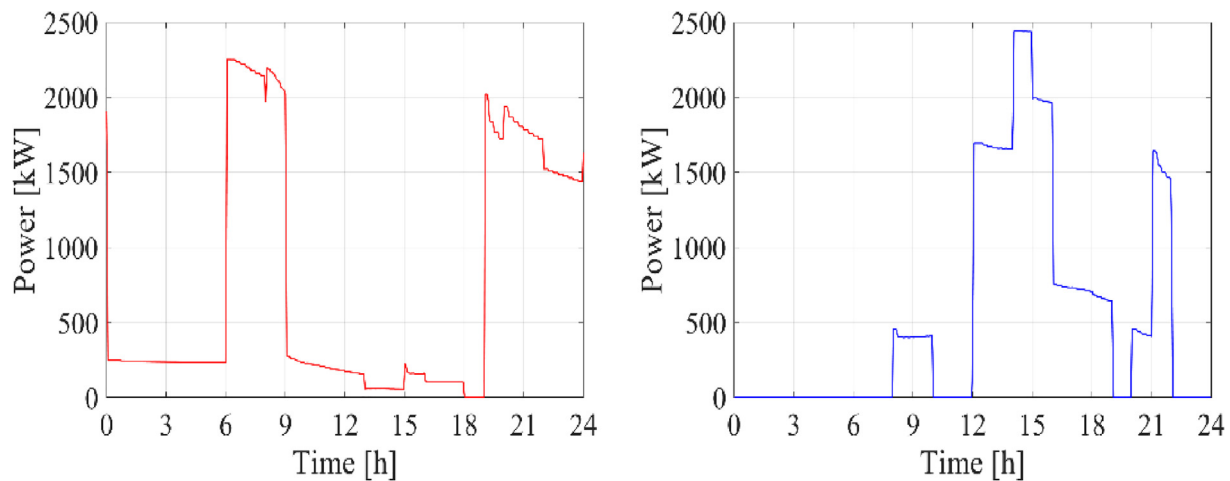


Fig. 4. Salina district thermal energy demand: heating (left) and cooling (right).

Table 2
Building simulation data.

Building element	Building			
	U-value [W/m ² K]	Thickness (m)	ρ_s (-)	ϵ (-)
Roof	1.086	0.340	0.4	0.9
Facades	1.404	0.380		
Ground floor	1.115	0.460		
Adjacent ceiling	1.792	0.290		
Windows glass	2.89	0.004/0.016/0.004	0.13	0.18

Table 3
Number of occupied district buildings, Santa Maria di Salina and Favignana.

Type of Building	Number of buildings			
	Summer-Period (May-September)		Winter-Period (October-April)	
	Salina	Favignana	Salina	Favignana
V1	378	344	155	280
V2	285	123	122	71
Off	16	10	16	10
H	20	20	2	2
Sch	0	0	3	2

power is delivered to the local grid if the production overcomes the demand. Note that the cooling loop of ACH and ECH is based on the seawater withdrawn by the thermocline (T_{SW} equal to 15 °C, Table 5).

The design of the area of the CPVT collectors, equal to 4800 m² (Table 4) is carried out considering results of the simulation of the reference buildings. In particular, in a preliminary analysis, the peaks of the demand are calculated. The peak of the demand for space heating and desalination during winter is 3.18 MW, whereas the peak of demand for the supply of the ACH and desalination is 4.48 MW; the peak of electricity demand is 0.92 MW. Considering the maximum heating demand and thermal efficiency of CPVT equal to 50%, the solar field area results in 8960 m². Considering the maximum electricity demand and electric efficiency of CPVT equal to 20%, the solar field area results in 4620 m². In the first system, it is assumed that the value of 4800 m² is the most plausible, but it is necessary to perform a sensitivity analysis to optimize the design.

The MED unit is designed to be supplied with 50 kg/s of hot water. Considering an inlet/outlet temperature difference of about 5 °C, the required heat demand of the process is 1 MW. Therefore, the capacity of AH for supporting the MED activation without solar energy is 1.2 MW

(Table 4). The capacity of AHs for DHW and space heating is selected in order to cover the maximum peak.

Proposed system PS2: PV-REV HP-RO regards Santa Maria di Salina and consists of a district heating/cooling network based on two reversible water-to-water HPs AERMEC WFG9613 [39]. The rated heating and cooling power of the HPs are equal to 1.8 MW and 1.7 MW with rated coefficient of performance (COP) of 4.14 and 4.85, respectively [39] (Table 5). The capacity of the heat pumps is selected by taking into account the peak of demand for heating and cooling equal to 2.25 MW and 2.85 MW, respectively. DHW is provided by a district heating network supplied by two water-to-water HPs AERMEC WFG4812 [39] with a rated heating power of 1.0 MW (Table 5). The cooling loop of each HP is based on the seawater withdrawn from the sea thermocline. Freshwater is produced by a RO equipped with SW30ULE-440i membranes [40]. In particular, the train consists of three pressure vessels with eight membranes each. The electricity demand of the district including the electric energy needed for the activation of RO unit and HPs is matched by a PV field of 9333 m². The area of the PV is selected in order to cover the maximum required power peak. The selection of the RO capacity is selected by considering that the RO production must cover 70% of the maximum freshwater demand. Note that when the produced solar power is not high enough for matching the electricity demand of the district, the electricity is withdrawn from the local grid of the island. When the power production is greater than the demand, the surplus is delivered to the grid of the island.

The main economic, energy and environmental assumptions to perform the dynamic simulations are reported in Table 6.

5. Results

In this section, the hourly, weekly and yearly results of the dynamic simulations for the two developed case studies of the two investigated layouts (PS1: CPVT-ACH-MED, PS2: CPVT-ACH-MED) in Salina and Favignana are presented. The developed simulation tool allows one to mimic the real time operation of the investigated systems, using hourly weather data of the selected locations. Dynamic results can be also integrated on other time bases (e.g. days, weeks, etc), in order to calculate the related energies and water mass. The dynamic simulations account for freshwater, heating, cooling and DHW hourly demand and the hourly values of the weather parameters of the islands, with a simulation time step equal to 0.025 h. A sensitivity analysis, performed to select the best configuration of the investigated plants from the economic and energy point of view, is also presented.

Table 4
Proposed system 1 (PS1), Favignana.

Component	Parameter	Description	Value	Unit
CPVT	N_{SC}	Number of CPVT collectors	400	–
	A_{CPVT}	CPVT aperture area	12	m^2
	v_{tk}	Specific tank volume	20	l/m^2
	$T_{set,WS}$	CPVT outlet setpoint temperature WS	60	$^\circ\text{C}$
	$T_{set,SS}$	CPVT outlet setpoint temperature SS	90	$^\circ\text{C}$
MED	M_{motive}	Nominal mass flow rate of motive hot water	$1.8 \cdot 10^5$	kg/h
	$T_{set,MED}$	MED rated inlet temperature	75	$^\circ\text{C}$
	T_{intake}	Temperature of seawater at intake facilities	25	
	$A_{sensible}$	Sensible heat transfer area at 1st effect	10	m^2
	A_{latent}	Latent heat transfer area at 1st effect	50	
	A_i	Heat transfer area in effects from 2 to 8	80	
	$A_{condenser}$	Heat transfer area at the condenser	62	
	C_t	Thermal capacity	1000	kW
	X_f	Salinity of feed water	38,000	ppm
	X_B	Maximum salinity of disposed brine	72,000	
	\dot{M}_{CW}	Mass flow rate of cooling water	$24 \cdot 10^3$	kg/h
ACH	N_{EFF}	Number of effects	11	–
	$P_{th,ACH}$	Rated cooling power	3.56	MW_{th}
	COP	Rated coefficient of performance	0.8	0.8
	$T_{set,ACH}$	Set-point temperature for the chilled water	7	$^\circ\text{C}$
Chiller	$P_{th,chiller}$	Rated cooling power	3.56	MW_{th}
	COP	Rated coefficient of performance	5.8	0.8
	$T_{set,chiller}$	Set-point temperature for the chilled water	7	$^\circ\text{C}$
AH (MED)	$P_{th,AH,MED}$	Rated auxiliary heater power	1.20	MW_{th}
AH (HEATING)	$P_{th,AH,heat}$	Rated auxiliary heater power	3.14	MW_{th}
AH (DHW)	$P_{th,AH,DHW}$	Rated auxiliary heater power	0.90	MW_{th}

5.1. Annual results

The annual results of the simulations (from January 1st to December 31st) reporting the integrated power and obtained freshwater production for PS1 and PS2 are summarized in Tables 7 and 8, respectively. Table 9 presents the annual energy, environmental and economic results of both PSs. Note that PS1 and PS2 include thermal- and electrically-driven solar technologies, respectively. Tables 7 and 8 show the fraction of solar thermal energy production of the CPVT collectors (PS1) and the fraction of the solar electric energy production of the PV panels (PS2) used for district space heating and cooling, for the production of DHW, freshwater, and electricity. In Table 7 the main thermal energies involved in PS1 are reported. One of the main technical parameters showing the performance of the system is the amount of solar thermal energy used for the different purposes, namely: heating, DHW, cooling and freshwater. For the simulated system, only a certain amount of the energy and water demand is matched by the solar energy. The rest is obtained by the auxiliary devices (heaters and chillers). Obviously, the amount of user demand covered by solar energy depends on the time-dependent combination of user demand and solar energy availability. This is shown in the last four columns of Table 7, reporting the solar fractions related to the heating, DHW, cooling and freshwater production subsystems of PS1. As expected, the lowest solar fraction equal to 13% is achieved for the heating subsystem, due to the significant mismatch between the solar thermal energy production and space heating demand in winter. This occurs mainly because the CPVT collectors, that convert only the beam radiation, show poor thermal performance during winter, due to the low beam-to-total radiation ratio. As a consequence, the proposed system is not expected to cover the space heating demand even in locations where this demand is significantly low, as for the cases of the two selected islands. However, this circumstance does not limit the goal to achieve a fully renewable system, since the auxiliary heat is provided by biomass boilers. The subsystem of the freshwater production reaches a solar fraction of about 25%. This is due to the fact that solar thermal energy is used primarily for space heating and cooling and DHW demands. When these loads are fully satisfied, solar energy is switched for the production of freshwater.

Therefore, for long periods (when TK2 temperature is below the set-point set for the activation of the MED system), the desalination unit is not supplied by solar energy and it is fully supplied by biomass auxiliary heater. The cooling subsystem shows a good solar fraction, about 56%. This is due to the simultaneity between solar energy availability and space cooling demand. In fact, summer CPVT solar thermal energy production is extremely high due to the high beam-to-total radiation ratio achieved in this period of the year. Considering the whole year, the solar fraction for the DHW subsystem is about 76%. This result is mainly due to the operation outside the heating and cooling season. In that period no space cooling and heating demand and solar energy is used to fully supply DHW demand. As for PS2, Table 8 shows that the total electricity consumption of the district and plant (4395 MWh/y), the electricity consumption of the RO unit (123 MWh/y), of the HP for DHW (388 MWh/y), and the HP for heating and cooling (385 MWh/y). It is worth noting that in PS2 all the energy and water demands are supplied by electricity. This system is much more flexible and easy to manage with respect to PS1, since the management of electricity among the different users is significantly easier compared to the case of thermal energy. The higher electricity production of the PV panels is due to the higher capacity of the solar field (9333 m^2), with respect to the CPVT collectors (4800 m^2), even though the CPVT collectors have a higher efficiency (20% vs 17%). The total electricity produced by the PV panels fails to cover the electricity demand of the district and RO unit, also because no energy storage system is included. This is due to the significant mismatch between solar energy availability and user demand. However, an electricity storage system is not considered in the present study due to the large capacity of the system and to the high capital cost of this device. Therefore, during the night hours, the electricity is always purchased from the grid. The ratios between self-consumed electricity and electricity produced by the PV panels to electricity demand are equal to 64% and 41%, respectively. Good performances are obtained for both PSs in terms of freshwater demand: the RO unit produces 68% of the freshwater demand of Salina, whereas the MED subsystem produces 59% of the freshwater demand of Favignana. PS2 reaches excellent performance in terms of SPB, PES and ΔCO_2 : equal to 3.3 years, 64.4% and 63.9%, respectively.

Table 5
Proposed systems 2 (PS2), Santa Maria di Salina.

Component	Parameter	Description	Value	Unit
PV (PS2)	P_{max}	Maximum power	260	W _p
	V_{oc}	Open-circuit voltage	37.7	V
	I_{sc}	Short-circuit current	9.01	A
	V_{mpp}	Voltage at point of MPP	30.5	V
	I_{mpp}	Current at point of MPP	8.51	A
	N_s	Number modules in series	2	–
	N_p	Number modules in parallel	2900	–
	A	PV module area	1.6	m ²
	N_{cell}	Number cells in series	15	–
	η_{PV}	Module efficiency	15.8	–
HP heat and cool (PS2)	$P_{th,HP,heat}$	Rated heating power	1.8	MW _{th}
	$P_{th,HP,cool}$	Rated cooling power	1.7	MW _{th}
	COP	Coefficient of prestation	4.14	–
	EER	Energy Efficiency Ratio	4.85	–
	T _{sw}	Temperature sea wataer	15	°C
HP DHW (PS2)	$P_{th,HPDWH}$	Rated heating power	1.0	MW _{th}
	COP	Coefficient of prestation	3.25	–
	T _{sw}	Temperature sea wataer	15	°C
RO (PS2)	$N_{membranes}$	Number of membranes for single train	24	–
	$N_{vessels}$	Number of vessels for single train	3	–
	N_{Trains}	Number of trains	1	–
	$A_{membranes}$	Active area of single membrane	41	m ²
	c_f	Salinity feed seawater	39	g/l
	$T_{seawater}$	Operation seawater temperature	12–29	°C
	η_{LPP}	Efficiency of low-pressure pump	0.85	–
	η_{HPP}	Efficiency of high-pressure pump	0.85	–
	η_{PX}	Efficiency of pressure exchanger	0.95	–
	$P_{r,lim,min}$	Limit pressure value ($P_{el,limit}$ condition)	42	bar
	$P_{r,rated}$	Rated pressure value (rated condition)	58	bar
	\dot{W}_{rated}	Rated flowrate RO unit	350	m ³ /h
	W_{tot}	Total yearly capacity	131,400	m ³ /year

As for the calculation of the cost of the network, it is found that the building density of the region of Santa Marina Salina is 1521.4 buildings/km² calculated for 852 buildings of mean surface area of 138 m² in a built area of 0.56 km², where the buildings are concentrated. The heat and cooling generation of the district heating and cooling network is a total of 1903 MWh/year, while that of the hot water district system generation is 1552 MWh/year. The two district networks are identical. The length of the tube per building is calculated to be 16 m with a pipe diameter of 35 mm, and a total pipe length of the network of almost 14 km. The capital expenditure of the piping network is estimated at 3.7 M€ [45], using the constants for outer city areas: C1 = 214 €/m and C2 = 1725 €/m² [35]. The island of Favignana includes 898 buildings of mean surface area of 119 m². The built area of the island is estimated at around 5 km², while it is assumed that 80% of the buildings of the island are concentrated in an area of 1.5 km² in the center of the island. The total heat and cooling demand of the island, covered by the district heating and cooling network, is 2322 MWh/year, while the thermal energy of the hot water district network for supplying the required hot water demand is 1440 MWh/year. The piping systems of the two district heating networks are identical. Under these calculations, the length of the tube per building is estimated at 27.9 m, resulting in a total network pipe length of 25 km. In this case, the capital expenditure of the piping network was found to be 8 M€, using the constants for

rural areas: C1 = 151 €/m and C2 = 1378 €/m² [35]. The investment in this case is found to be approximately double that of the case of Santa Marina Salina, mainly due to the more scattered buildings over the surface area of the island.

The economic feasibility of PS2 is good, mainly due to the present low capital cost of PV panels, compared to the extremely high capital cost of CPVT collectors (Table 6). This is a remarkable result, considering the high cost of the piping network. On the other hand, the economic feasibility of PS1, is poor (Table 9) due to the huge capital costs for the district heating network. Similar economic results were obtained for PS1 with layouts including CPVT collectors, with SPB equal to 12.5 [14] and 13.6 [25] without any economic incentive, where the costs of the piping network were not considered. The PES and the avoided emissions ΔCO_2 of PS1 are also lower than those reached for PS2, 32.2% and 27.8%, respectively. This is due to the high electricity demand in the proposed system, mainly covered by the grid with a low efficiency and to the high thermal energy demand covered principally by the auxiliary heater during winter.

5.2. Weekly results

In order to better comprehend the trends of the main energy fluxes over the seasons of year, the aggregated results of PS1 and PS2 are reported in Figs. 6 and 7 on a weekly basis. In PS1, the thermal energy demand for DHW is covered from the solar tank TKdhw, for most of the year. In fact, as shown in Fig. 6, approximately between the 13th and the 18th week, the auxiliary heater is switched off. This occurs because during these weeks the thermal energy demand for space heating and cooling of the district is null and all of the produced thermal energy with the CPVT collectors is used for DHW purposes. This circumstance also justifies the results reported in the previous sections, dealing with the yearly integrated results. In fact, in those weeks solar energy can be used mainly for DHW purposes and desalination. Conversely, the thermal energy of the AH is significant during summer, because the thermal energy produced with the CPVT collectors is used to supply the ACH. In that period of the year the CPVT efficiency and solar availability is high, resulting also simultaneous with the space cooling demand. The tank TK2, $E_{th,TK2}$, is not able to cover the energy demand of the MED unit, $E_{th,MED}$, the first and the last weeks of the year, corresponding to the winter season: therefore, the auxiliary heater is activated to match the MED energy demand. In fact, in winter solar energy is mainly used for space heating purposes since this demand is significantly higher than solar availability, as mentioned in the previous section. During winter, the space heating energy demand, $E_{th,heat,dem}$, is quite high, reaching about 125 MWh the first weeks of the year. Conversely, solar thermal production is low to the low beam radiation available in winter. Then, it decreases until the end of the heating season, March 31st, due to the mild climate of the island of Favignana. The solar thermal energy, $E_{th,TKheat}$, of the tank TKheat covers only a small part of the district demand. In particular, it reaches its peak on the 12th week of the year (March), due to the increase of the radiation availability and, thus, the solar thermal energy production. Space cooling energy demand, $E_{th,cool,dem}$ (Fig. 6) is required intensely between weeks 25 and 40 and its peak is reached at the end of August. $E_{th,TKcool}$ of the tank TKcool can cover the cooling energy demand at the beginning and at the end of the cooling season, whereas in the middle of the season, the demand is partially covered by the electrical chiller ECH ($E_{th,ECH}$).

Fig. 7 shows the weekly electric energy production of the PV panels, $E_{el,PV}$, the total electric energy supplied to the RO unit, Salina district, and auxiliary components of PS2 $E_{el,RO+District+Aux}$, the electric energy withdrawn from the grid, $E_{el,fromGRID}$, and supplied to the grid, $E_{el,toGRID}$, and the total electricity supplied to the HP for DHW, space heating, and cooling, $E_{el,HPheat+cool+DHW}$. $E_{el,PV}$ reaches maximum values during summer. However, in these same summer weeks, a greater electricity demand of the district is noted, due to the increase of the tourists.

Table 6

Thermoeconomic and environmental assumptions.

Parameter	Description	Value	Unit
C_{CPVT}	CPVT unit capital cost per m ² of solar field	600	€/m ²
C_PV	PV unit capital cost per kW _{el}	1000 [37]	€/kW _{el}
$C_{HP\ H\&C}$	Cost heat pump heat and cool	541.5 [39]	k€
$C_{HP\ DHW}$	Cost heat pump heat and cool	512.7 [39]	k€
C_{PrVess}	Cost of pressure vessel for 8-inch elements	1.2 [41]	k€/vessel
$C_{membrane}$	Windows replacement cost per m ²	889.58 [42]	€/membrane
C_{piping}	Cost of piping (small size train)	113.5 [41]	k€/RO train
C_{frame}	Cost of support frame	70[41]	k€/RO train
$C_{instrument}$	Cost of instrument and control (whole plant)	28 [41]	k€
$C_{ship\&inst}$	Cost of shipping, handling, installation and insurance	15 [41]	%
C_{pump}	Cost of RO variable speed pumps	7.75 [10]	k€
C_{PX}	Cost of Pressure exchanger	64 [43]	k€/PX
$C_{AH,aux}$	Cost of Auxiliary heater	89	€/kW _{th}
$C_{chiller}$	Cost of Electric chiller	150	€/kW _{th}
C_{ACH}	Cost of Absorption chiller	$C_{ACH} = 10^{-5}P_{th,ACH}^3 - 0.0393P_{th,ACH}^2 + 244.53P_{th,ACH} + 95.494$	€
C_{HE}	Cost of Heat exchanger	$C_{HE} = (A_{HE}/0.093)^{0.75}$	€
C_{MED}	Cost of MED capital	$C_{MED} = 0.5[300(A_{MED})^{0.95} + 800(86.4M_{fresh})]$ [25]	€
C_{TK}	Cost of the tank	$C_{TK} = 494.9 + 808.0 \cdot V_{TK}$ [13]	€
$C_{pumpsSS}$	Cost of the small pumps (single speed)	$C_p = 1.08 \cdot (-2 \cdot 10^{-8} \cdot \dot{m}^2 + 0.0285 \cdot \dot{m} + 388.14)$ [10]	€
$C_{pumpsVS}$	Cost of the small pumps (variable speed)	$C_p = 1.08 \cdot (-2 \cdot 10^{-8} \cdot \dot{m}^2 + 0.0285 \cdot \dot{m} + 388.14) + 1000$ [10]	€
$J_{el,fromGRID}$	Electric energy purchasing unit cost	0.18	€/kWh
$J_{el,toGRID}$	Electric energy selling unit cost	0.07	€/kWh
J_{NG}	Natural gas unit cost	0.88	€/Sm ³
$J_{biomass}$	Wood chip unit cost	0.06	€/kg
$J_{water,ship}$	Cost of water supplied throughout tank-ship	7	€/m ³
m_{CPVT}	CPVT maintenance yearly cost	2	%/year
m_{RO}	RO unit maintenance yearly cost	2 [8,44]	%/year
m_{PV}	PV maintenance yearly cost	1.5	%/year
LHV_{NG}	Natural gas lower heating value	9.59	kWh/Sm ³
$LHV_{biomass}$	Wood chip lower heating value	3.7	kWh/kg
$\eta_{el,RS}$	Thermo-electric power plant efficiency for the local island grid	35	%
$\eta_{AH,RS}$	Natural gas auxiliary heater in reference system	80	%
$\eta_{AH,PS}$	Natural gas auxiliary heater in proposed system	95	%
$COP_{CH,RS}$	Electric chiller coefficient of performance	3	—
F_{NG}	Equivalent CO ₂ emissions for coefficient for natural gas	0.20	kgCO ₂ /kWh _{PE}
F_{el}	Equivalent CO ₂ emissions for coefficient for electric energy	0.48	kgCO ₂ /kWh _e
a	Discount rate	5	%
TH	Time horizon	20	years

It is clear that, the increase of the electricity demand during the hotter weeks also leads to peak values of electricity withdrawn from the grid, $E_{el,fromGRID}$, as well as a decrease of the electricity delivered to the grid, $E_{el,toGRID}$. Note that purchasing electric energy in layouts coupling PV fields with electric-driven technologies without electric storage systems, is necessary to cover the energy demand during the night hours, when the PV electric energy production is null. In addition, the growing trend of $E_{el,RO+District+Aux}$ during summer is due to the increase of the electricity demand of the district because the RO unit demand is almost constant during the year. A slight increase of energy delivered to the RO unit is detected in summer due to the longer days. The electricity consumed by heat pumps for space heating and cooling and DHW of the district, $E_{el,HPheat\&cool+DHW}$, is lower than the produced energy $E_{el,PV}$ from the 9th to the 33rd week, i.e., when the HP for space heating and cooling consumption is low and the $E_{el,HPheat\&cool+DHW}$ considers only the electric energy demand of the HP for DHW. Conversely, during the colder winter weeks and the hotter summers weeks, the $E_{el,HPheat\&cool+DHW}$ is higher than the produced energy $E_{el,PV}$. The weekly specific energy consumption, not shown for sake of brevity, is averagely constant equal to 2.1 kWh/m³, lower than the average value suggested in literature, equal to 3.3 kWh/m³ [13]. The reason for this difference is that in this layout the pressure exchanger is included.

5.3. Hourly results

In order to better understand and analyze the operation of the plants, in terms of temperature, power, and implemented control strategies, the hourly results of dynamic simulations are also discussed. In

particular, typical winter and summer operation days are investigated for the proposed systems PS1 and PS2.

In a typical summer day (Fig. 8), the outlet temperature of the CPVT collectors in PS1 is equal to 90 °C. The reported oscillating trend is due to the varying inlet water temperature, depending on the thermal load of the plant, slightly affecting the CPVT inlet temperature. Fig. 8 also shows the variation of the operation of the CPVTs as a function of the solar radiation. When the solar radiation is null, the feedback controller of the pump P1 stops the pump. The pump operates only when the radiation is not null and the outlet water temperature from the collectors is higher than the inlet water temperature, coming from the bottom part of the TK1 or TK2. The electrical and thermal efficiencies of the CPVT are equal to 20% and to 60%, respectively. The operation of PS1 in a typical summer day is shown in Fig. 9. The left graph presents the top TK1 and TK2 temperatures, $T_{top,TK1}$ and $T_{top,TK2}$, to show the implemented control strategy regarding the management of the thermal storages. The CPVT collectors first supply TK1, matching the cooling and DHW demand. Solar thermal heat is then delivered to TK2, supplying heat to the MED unit, only when TK1 is fully charged i.e., when its top temperature reaches the set-point temperature equal to 86 °C. This occurs around midday, when the trends of $T_{top,TK1}$ and $T_{top,TK2}$ show the continuous switching of the CPVT outlet hot water between the two tanks. In particular, from 09:00 to 13:00, the thermal energy required by the auxiliary heater, supporting the MED activation, decreases considerably. This is also due to the trend of the Favignana district cooling demand, which is negligible during these hours (Fig. 5), in comparison to the cooling demand during the afternoon hours. In fact, from 12:00 to 17:30, all the solar heat is delivered to the TK1, supplying

Table 7
Annual results: Proposed System 1 (PS1).

Eel,CPVT MWh/y	Eth,CPVTP %	Eth,MED	Eth,TKheat	Eth,TKdhw	Eth,TKcool	Eth,TKheat/(Eth,TKheat + Eth,AH)	Eth,TKdhw/(Eth,TKdhw + Eth,AH)	Eth,TKcool/(Eth,TKcool + Eth,AH)	Eth,MED/(Eth,MED + Eth,AH)
1240	3180	1100	168	1080	577	13	75	56	25

Table 8
Annual results: Proposed System 2 (PS2).

E _{el,PV}	E _{el,RO}	E _{el,District& plant&RO}	E _{el,HPheat}	E _{el,HPdhw}	E _{el,HPcool}	E _{el,self/} E _{el,demand}	E _{el,self/} E _{el,prod}
MWh/y						%	
2820	123	4395	201	388	184	41	64

Table 9
Annual energy, environmental and economic results: PS1 and PS2.

PS1	PS2	PS1	PS2	PS1	PS2	PS1	PS2
PE _{RS} [MWh/y]		PES [%]		ΔC [k€/y]		FW _{PROD} /FW _{demand} [%]	
15,575	13,600	32.2	64.4	490	1265	59	68
ΔCO ₂ [%]		J _{tot} [M€]		SPB [years]		PI [-]	
27.8	63.9	13.8	7.84	28.2	6.2	-	0.5

the ACH for the chilled water production. Due to the high cooling demand of the district, $T_{top,TK1}$ significantly decreases from 86 °C to 75 °C. $T_{top,TK1}$ increases again up to 85 °C when the cooling demand decreases around 18:00. As it can be seen, in the early morning and afternoon hours the freshwater is obtained only by the auxiliary heater without any solar energy support.

The production of freshwater has a constant trend (Fig. 10) of almost 15 m³/h, but the summer freshwater demand is higher than the production, especially in the morning and evening hours. The stable water production is due to the constant supply water temperature of the MED unit. In particular, the plant is equipped with a biomass auxiliary heater AH (switching on only when the radiation is not null, from 06:00 to 18:00) that allows constant activation temperature of 75 °C of the MED unit, when the top temperature TK2 is lower than 75 °C. The graphs also show that during the selected day, AH is always activated. Note that during summer, freshwater demand is high due to the large number of tourists on the island of Favignana and, as it occurs in the day represented in this figure, the system is not able to cover the freshwater demand of the users. Therefore, it is necessary to purchase freshwater from the mainland (by ships) at high cost (7 €/m³). This result affects the profitability of the plant in a negative manner. The cooling demand is almost covered for all hours of the day by the chilled water produced by the ACH (driven with solar thermal energy) and stored into TKcool. It is thus possible to take advantage of the thermal inertia of the tank until 20:30, while, after this time, the activation of the auxiliary electric chiller is needed. Nevertheless, this only occurs for a small number of hours and for covering a small amount of the cooling demand due to the considerably decreasing of the ambient temperature in the evening hours.

When the ambient temperature T_{amb} decreases, the heating demand (Fig. 11) of the district is significant. This occurs during the first hours of the day, when the top temperature of storage tank TKheat is lower than the set point temperature of the water in the direction of the district buildings (equal to 55 °C). At that point, the auxiliary burner $P_{th,AH}$ is switched on to cover the heating demand. Around midday, T_{amb} increases up to about 20 °C, the heating demand decreases and the storage tank TKheat covers the demand until it is discharged. This occurs from 09:00 to 20:00, when the AH gets reactivated. Regarding the DHW demand, it is possible to note that in a typical spring day, when both heating and cooling demand are null, the storage tank TKdhw covers all of the user demand.

In Fig. 12 the trends of power generation and demand for a typical summer day during the operation of PS2 are presented.

During the night hours, when the radiation is null, because no electric storage system is included in the proposed layout, the electric demand of the users is matched by the local pre-existing grid of the district of Santa Marina Salina (at 0.18 €/kWh_e). PV production reaches a peak value of 1.1 MW at midday. Between 09:00 and 15:00, the

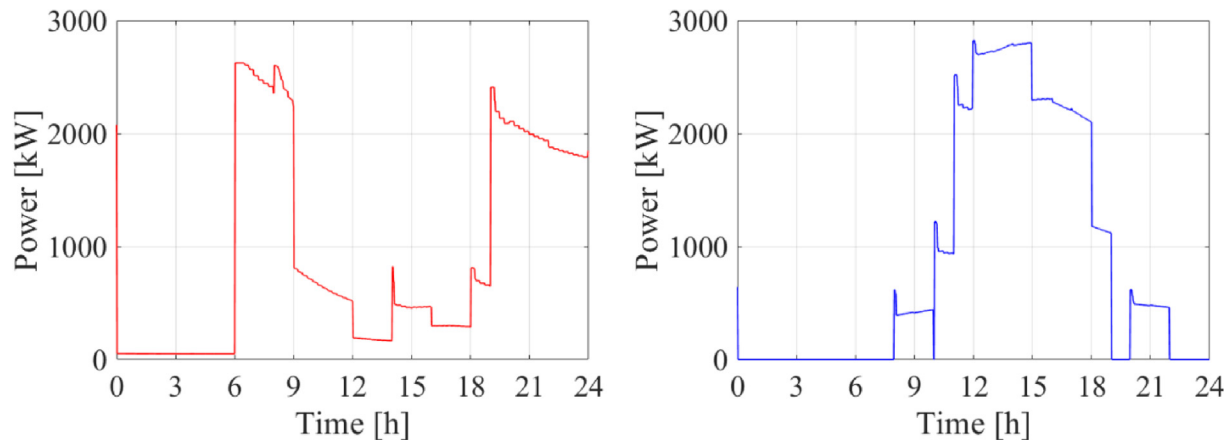


Fig. 5. Favignana district thermal energy demand: heating (left) and cooling (right).

electricity demand, including the electricity demand of Salina district and the electricity for the plant and RO unit, is lower than the electricity production of the PV panels. In fact, as it is possible to see, during these hours, PV panels completely satisfy the electric demand without using electricity of the local grid. The surplus of the power production is delivered to the local grid at 0.07 €/kWh. When the RO unit turns on, an initial transient trend of the production is noted, followed by a stable freshwater production, equal to 13 m³/h. It is possible to note that the desalination unit only works during daytime.

5.4. Sensitivity analysis

For both PSs, a sensitivity analysis is performed in order to evaluate the effect of the variation of the main design parameters of the plant on the system profitability. In particular, one of the key aspects in the design of those plants is the selection of the capacity of the components. In the initial design discussed above, solar field capacities were selected in order to achieve a reasonable solar fraction, according to values suggested by many published papers. Similarly, for the desalination

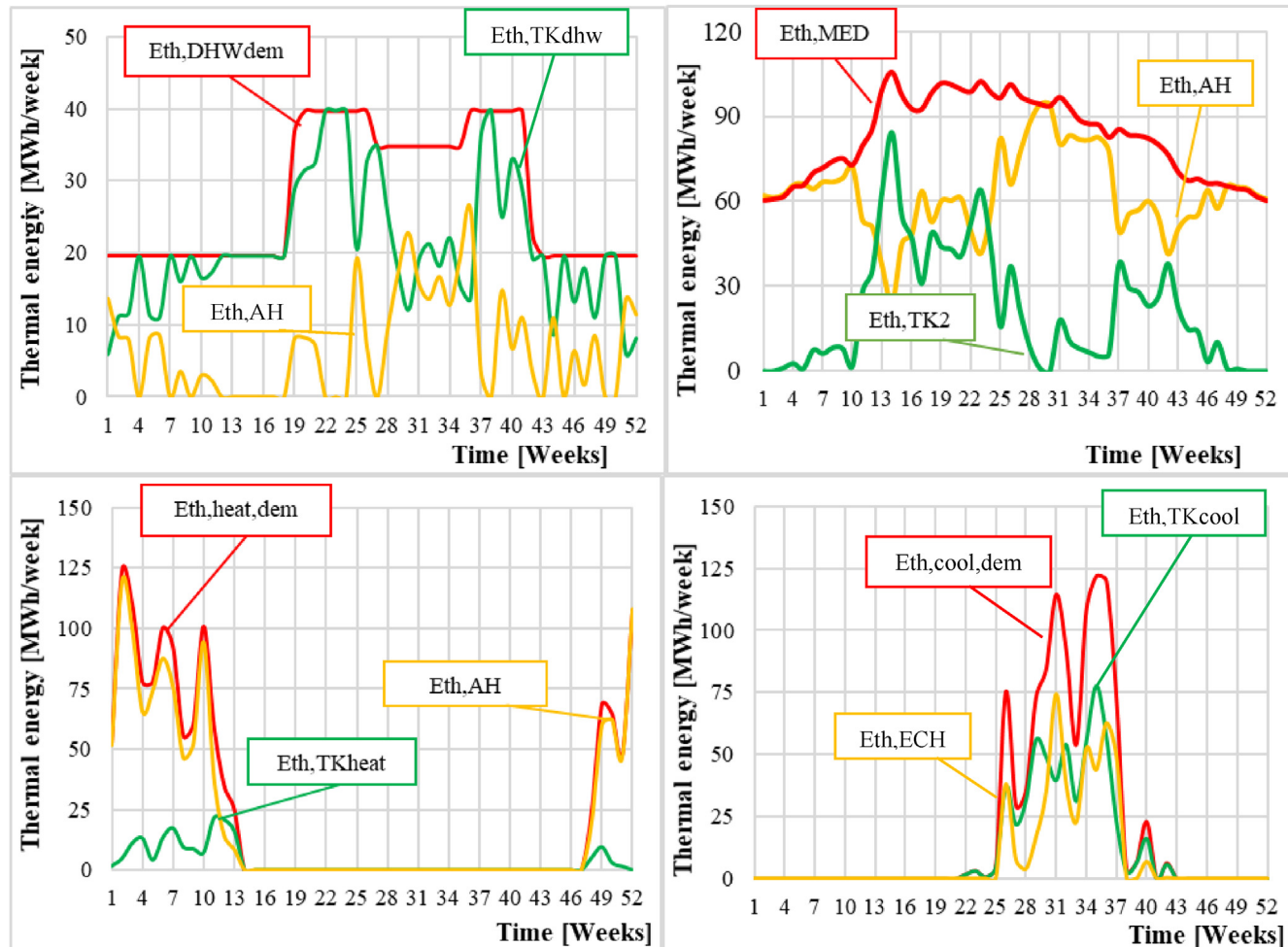


Fig. 6. Proposed System 1 (PS1) Weekly results: thermal energy.

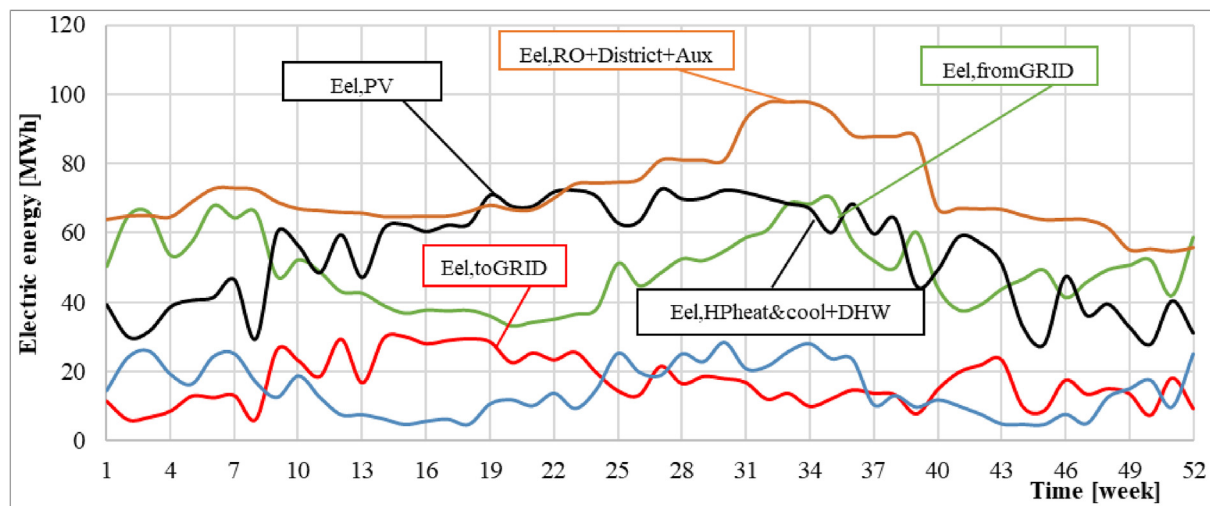


Fig. 7. Proposed System 2 (PS2) Weekly results: electric energy.

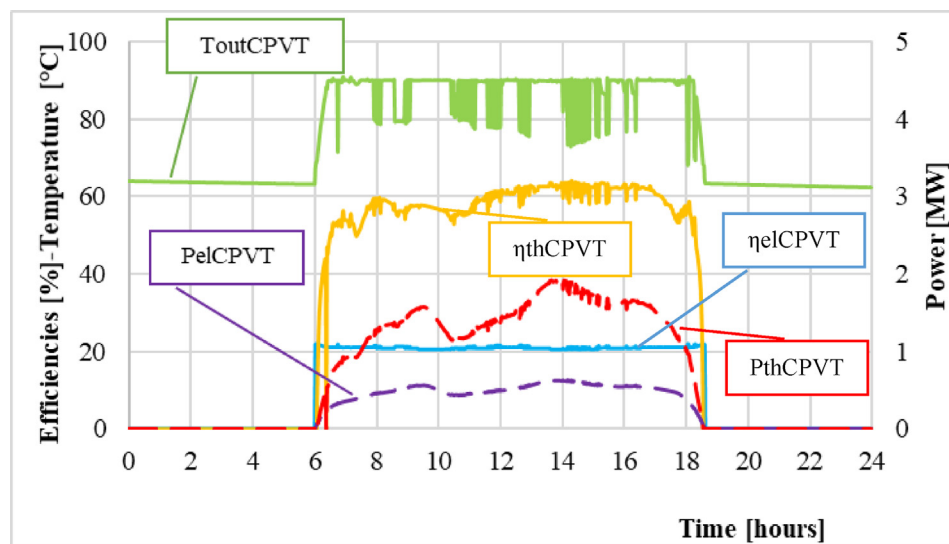


Fig. 8. Proposed System 1 (PS1). A typical summer day (solar collectors).

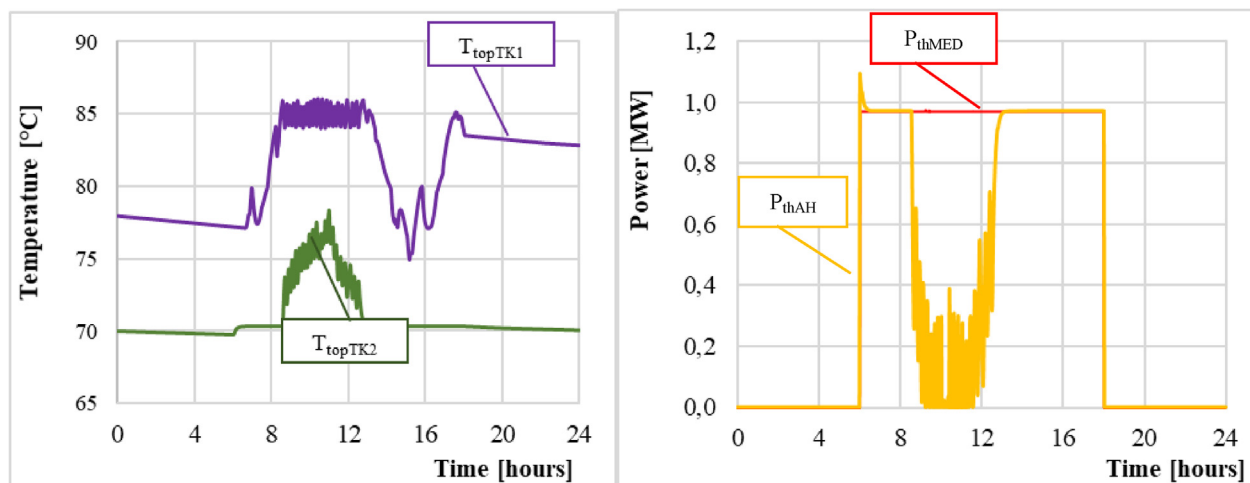


Fig. 9. Proposed System 1 (PS1). A typical summer day, tanks TK1 and TK2 temperatures (left), auxiliary heater (AH) and desalination unit (MED) power (right).

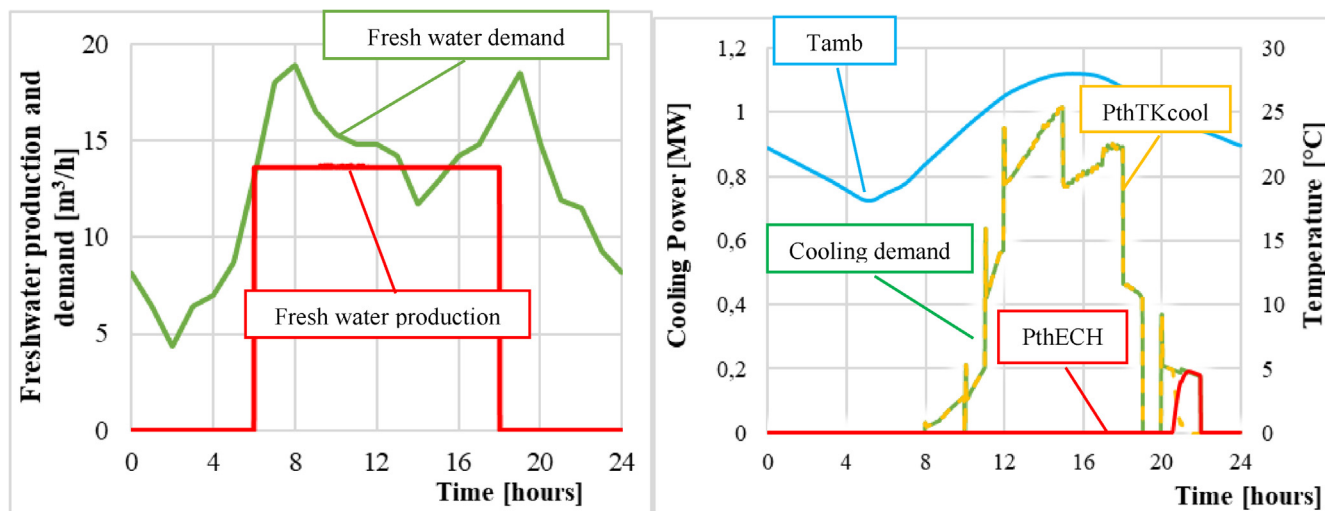


Fig. 10. Proposed System 1 (PS1). Summer day: Freshwater and cooling production and demand.

units, their capacity is selected to match most part of the freshwater demand. The selection of these capacities is not trivial. In fact, from an energy point of view, the designer should select the highest possible capacities (for both solar and desalination subsystems). From an economic point of view, on the other hand, the higher the capacity, the higher the capital cost and the possible savings in terms of operating costs. To assist the designer in this selection, this work includes a sensitivity analysis, varying the following parameters:

- the area of MED effects N_{EFF} , from 5 to 14 in PS1;
- the area of the PV field A_{PV} , from 5000 to 25,000 m² in PS2.

With the increase of N_{EFF} (Fig. 13) a slight growing trend of the freshwater production is obtained. This implies that a greater amount of the freshwater demand is covered by solar desalination. In particular, if N_{EFF} increases from 5 to 14, the freshwater demand covered by the MED unit grows from 31% to 75%, with the related economic saving. According to the higher freshwater production, the economic saving ΔC also increases, and as a consequence, although the higher capital cost of the system, SPB decreases from 46 years to 23 years. Therefore, the analysis suggests to maximize the capacity of the desalination unit. This is mainly due to the high value, typical in remote islands, of the purchasing cost of freshwater, assumed in this analysis equal to 7 €/m³.

This additional income partly compensates the high cost of the district network. In other words, this result suggests that the production of freshwater is much more profitable than energy production.

In Fig. 14, the effect of the variation of the A_{PV} on the PS2 profitability is summarized. In particular, the ratios $E_{el,self}/E_{el,demand}$ and $E_{el,self}/E_{el,PV}$ are reported. Note that the first ratio represents the fraction of the self-consumed electric energy with respect to the total electric energy demand and the second ratio represents the fraction of the self-consumed electric energy with respect to the renewable energy production. With decreasing A_{PV} , $E_{el,self}/E_{el,demand}$ decreases, while for A_{PV} values higher than 13,000 m² no important increasing is noted. $E_{el,self}/E_{el,PV}$ increases dramatically with decreasing solar field area, up to 85.18% for an A_{PV} equal to 5000 m². This occurs because the reduction of A_{PV} leads to a reduction of the total electric energy production without excesses delivered to the grid. Conversely, the increase of the A_{PV} leads to an increase of the excess delivered to the grid, $E_{el,toGRID}$, at low selling unit cost, whereas the capital cost significantly increases. This leads to a slight rising trend of the SPB, up to 6.6 years, and a decreasing trend of PI (due to the higher weight of the increase of the plant capital cost J_{tot} with respect to the lower increase of the yearly economic saving ΔC , because the increase of the electric energy is transferred to the grid at low unit cost).

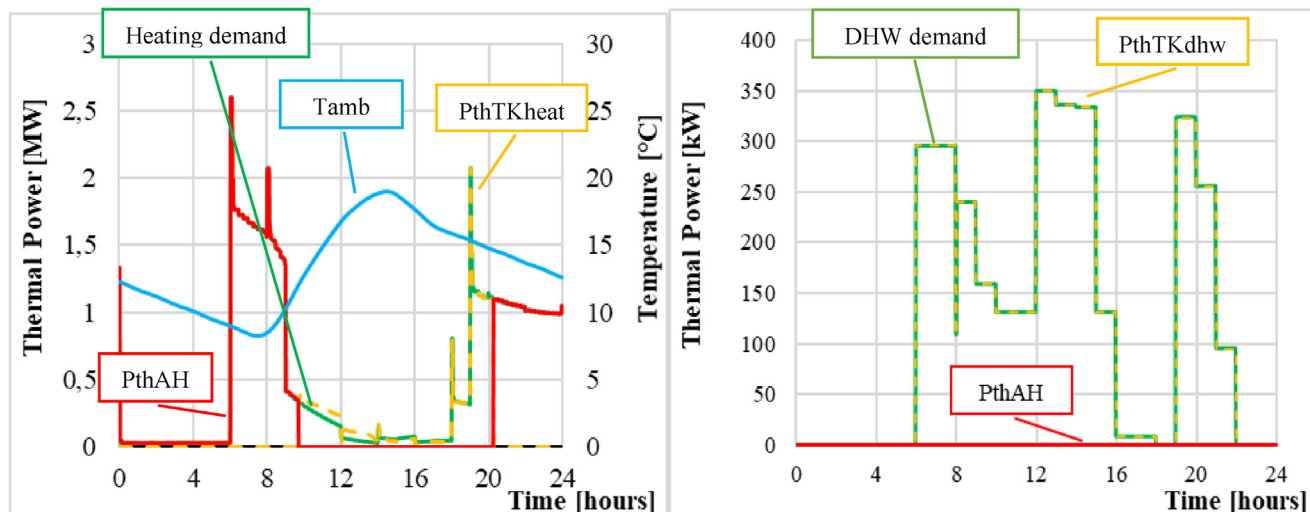


Fig. 11. Winter day: heating production and demand; Spring day: Domestic Hot Water (DHW) production and demand, Proposed System 1 (PS1).

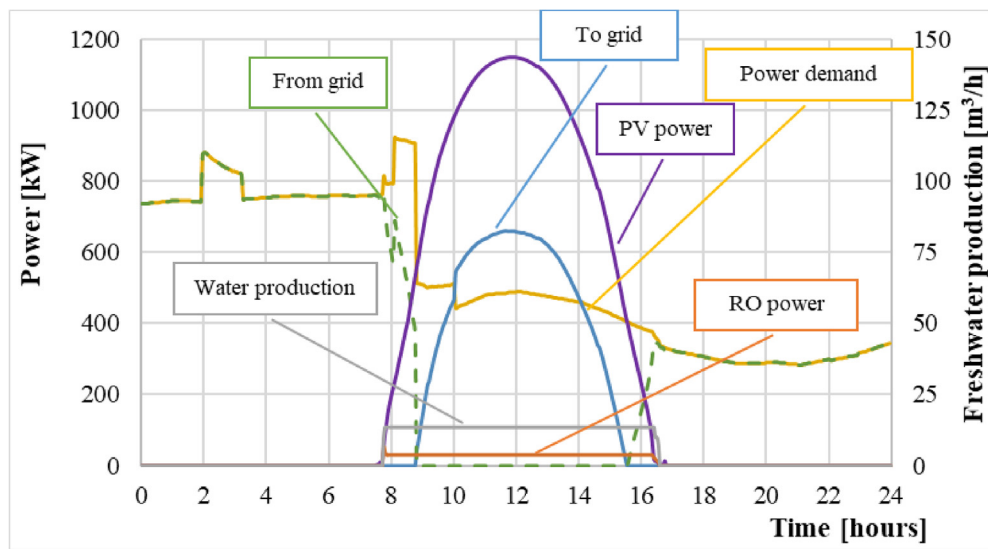


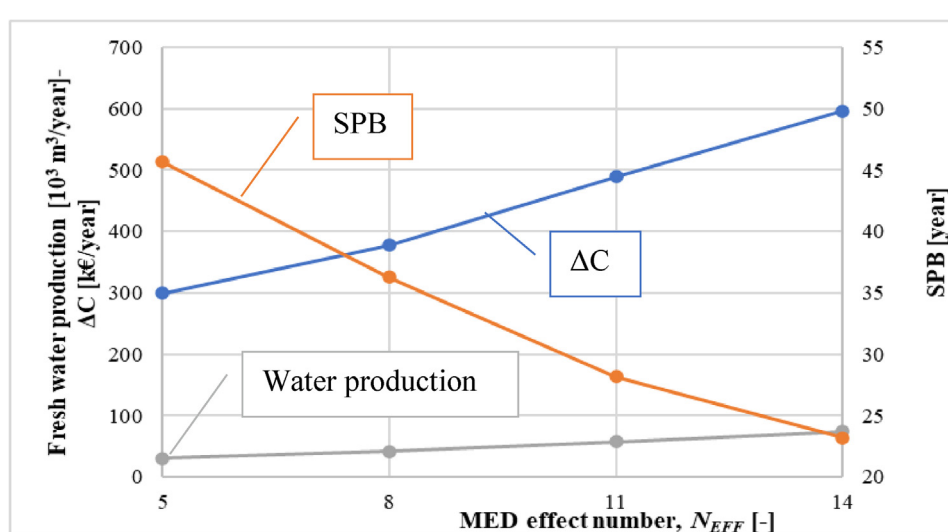
Fig. 12. Proposed System 2 (PS2). Summer day, main electrical fluxes.

6. Conclusion

This work presented the dynamic simulations of two solar poly-generation plants, consisted of thermally- and electrically-driven technologies for the production of freshwater, space heating and cooling, domestic hot water, and electricity. In particular, the first layout was based on concentrating photovoltaic and thermal collectors, an absorption chiller, and a multi effect distillation unit. The second layout was based on photovoltaic panels, heat pumps for space heating/cooling and domestic hot water, and a reverse osmosis unit. The investigated plants were modelled in TRNSYS and their energy, environmental and economic performance were evaluated. The two plants were designed to cover the energy demand of two different districts located on two islands of Sicily (South of Italy), in order to improve the decarbonization of their energy supply system, based only on the use of renewable energy. For all of the buildings in the districts, the hourly demand of freshwater, space heating and cooling, domestic hot water, and electricity were evaluated. Sensitivity analyses were performed by varying the capacity of the photovoltaic panel field and the number of the multi-effect distillation effects of the desalination unit. The results of the simulations for the first polygeneration plant were summarized in the following:

- during summer, the global efficiency of the concentrating photovoltaic and thermal field is satisfying, and the solar production covers a significant amount of the total energy demand, due to the high beam radiation;
- during winter, and due to the decrease of thermal and electrical efficiency of the concentrating photovoltaic and thermal collectors, the energy demand is almost totally covered by auxiliary heaters, mainly activated for the production of freshwater by the multi-effect distillation process and the district space heating;
- the obtained primary energy savings, avoided CO₂ emissions, and simple payback period were equal to 32.2%, 27.8% and 12 years, respectively;
- the sensitivity analysis suggests adopting a high number of multi-effect distillation effects. Even though the desalination system has a high capital cost, the payback period decreases when the effects of the distillation process increase from 5 to 14;
- the investigated plant, fully based on the use of renewable sources (solar and biomass), could be a reasonable investment in the future with the support of incentives.

The main results of the second polygeneration plant are:

Fig. 13. Proposed System 1 (PS1): Sensitivity analysis on the number of effects of the desalination units, N_{EFF} .

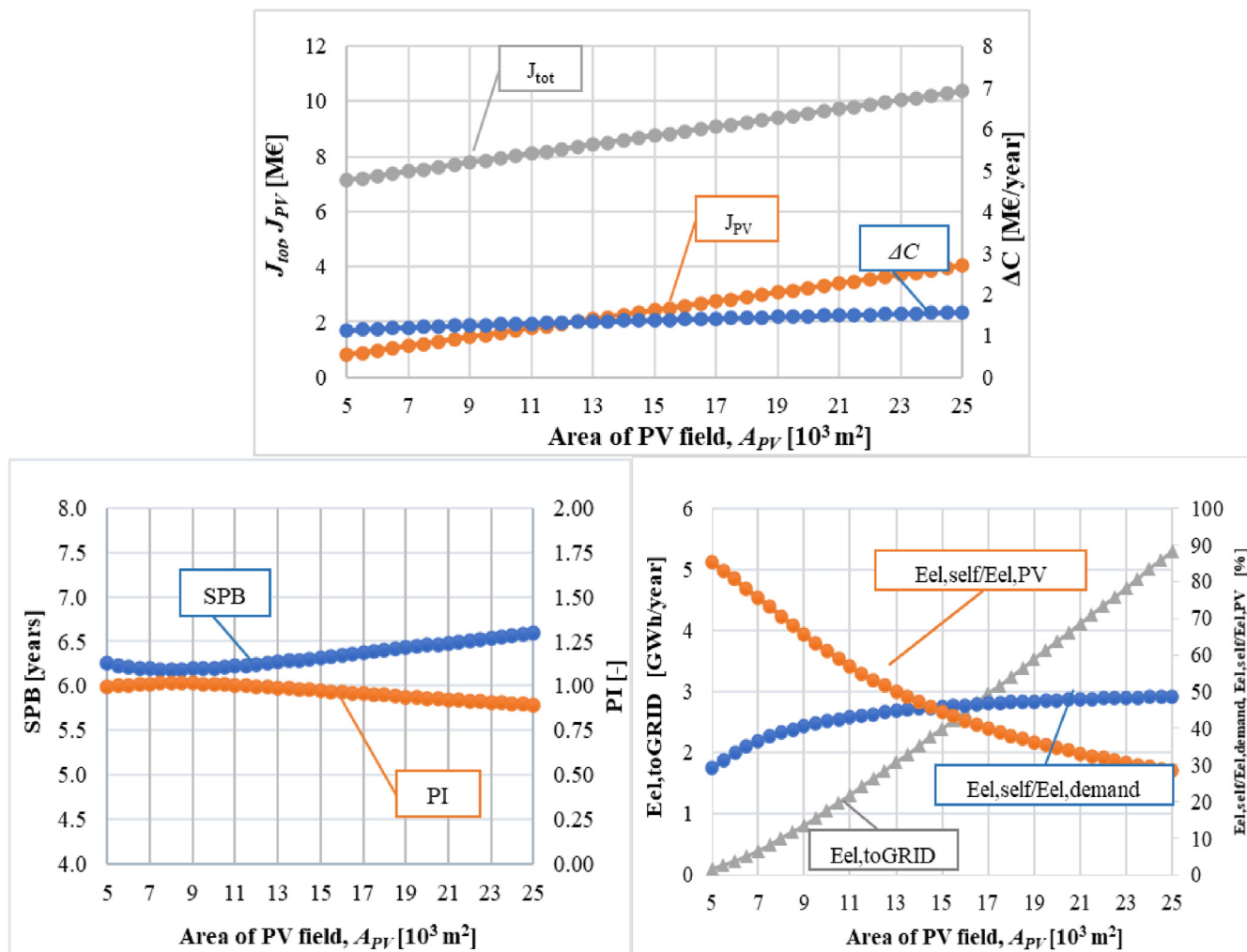


Fig. 14. Proposed System 2 (PS2): Sensitivity analysis of the photovoltaic field area, A_{PV} .

- the considerable advantages in terms of energy, environmental and economic savings: the obtained primary energy saving, avoided CO₂ emissions, and simple payback period are equal to 64.4%, 63.9% and 6.2 years, respectively. This is mainly due to the use of a heat pump, an established technology with high energy efficiency;
- with the adoption of electric storage systems, an improvement of the self-consumed electric energy could be attained, reducing the electric energy withdrawn from the grid during night hours;
- good performance is obtained in terms of freshwater demand: reverse osmosis unit produces 68% of the freshwater demand;
- the variation of the area of the photovoltaic field from 5000 m² to 25,000 m² suggests including a smaller photovoltaic field compared to the one studied, in order to increase the plant profitability.

The piping networks of the district heating and cooling systems of the two cases studies need to cover areas of relatively low energy demand. This is a result of the relatively high number of secondary homes or vacation houses and low occupation of a large number of buildings in the communities, especially in the winter. Nevertheless, these networks promote the incorporation of renewable energy in communities currently strongly dependent on fossil fuels, which would reduce the environmental impact of local energy and water generation.

Finally, the obtained results of this work, could be used as a reference for the self-sufficiency and decarbonization of other small Mediterranean islands, rich in renewable energy sources and seawater, featured by limited sources of fossil fuels and freshwater, and high

freshwater costs. The results of the paper show that some arrangements of renewable polygeneration systems are not currently profitable when compared with conventional fossil fuel systems. However, these systems are very promising for isolated islands. In fact, for islands featured by short offshore distance and stable load demand, the direct connection with mainland water and energy network is the most common option. However, in case of small islands which are furthest away from the coastline, the interconnection schemes are significantly complex and hybrid energy systems based on local RESs represent the best solution, for the production of both energy and water. Results are specially promising for those islands where buildings are located in small areas close to the coast, minimizing the cost of the district network. In the framework of the solar desalination technique, the performed thermoeconomic analysis model can help to guide the optimal plant location and the selection of design parameters, for the selected island.

Finally, the study confirmed that, in the current energy market, photovoltaic panels coupled with electric driven HPs are more profitable than concentrating photovoltaic and thermal collectors coupled with thermally-driven technologies.

Declaration of Competing Interest

The authors declare that they have no known competing financial interests or personal relationships that could have appeared to influence the work reported in this paper.

References

- [1] Calise F, et al. A novel renewable polygeneration system for a small Mediterranean volcanic island for the combined production of energy and water: Dynamic simulation and economic assessment. *Appl Energy* 2014;135:675–93.
- [2] Buonomano A, et al. BIPVT systems for residential applications: An energy and economic analysis for European climates. *Appl Energy* 2016;184:1411–31.
- [3] Calise F, et al. Transient analysis of solar polygeneration systems including seawater desalination: A comparison between linear Fresnel and evacuated solar collectors. *Energy* 2019;172:647–60.
- [4] Renne C, et al. Performance analysis of a CPV/T-DC integrated system adopted for the energy requirements of a supermarket. *Appl Therm Eng* 2019;149:231–48.
- [5] Buonomano A, et al. Transient analysis, exergy and thermo-economic modelling of façade integrated photovoltaic/thermal solar collectors. *Renew Energy* 2019;137:109–26.
- [6] Calise F, d'Accadida MD, Vanoli L. Design and dynamic simulation of a novel solar trigeneration system based on hybrid photovoltaic/thermal collectors (PVT). *Energy Convers Manage* 2012;60:214–25.
- [7] Tian L, Tang Y, Wang Y. Economic evaluation of seawater desalination for a nuclear heating reactor with multi-effect distillation. *Desalination* 2005;180(1):53–61.
- [8] Calise F, et al. Economic assessment of renewable energy systems integrating photovoltaic panels, seawater desalination and water storage. *Appl Energy* 2019;253:113575.
- [9] Calise F, d'Accadida MD, Vicidomini M. Optimization and dynamic analysis of a novel polygeneration system producing heat, cool and fresh water. *Renew Energy* 2019;143:1331–47.
- [10] Buonomano A, et al. A novel renewable polygeneration system for hospital buildings: Design, simulation and thermo-economic optimization. *Appl Therm Eng* 2014;67(1–2):43–60.
- [11] Calise F. Thermoeconomic analysis and optimization of high efficiency solar heating and cooling systems for different Italian school buildings and climates. *Energy Build* 2010;42(7):992–1003.
- [12] Calise F, et al. A novel solar-assisted heat pump driven by photovoltaic/thermal collectors: Dynamic simulation and thermoeconomic optimization. *Energy* 2016;95:346–66.
- [13] Buonomano A, et al. Adsorption chiller operation by recovering low-temperature heat from building integrated photovoltaic thermal collectors: Modelling and simulation. *Energy Convers Manage* 2017;149:1019–36.
- [14] Calise F, et al. Polygeneration system based on PEMFC, CPVT and electrolyzer: Dynamic simulation and energetic and economic analysis. *Appl Energy* 2017;192:530–42.
- [15] Kyriakarakos G, et al. Polygeneration microgrids: A viable solution in remote areas for supplying power, potable water and hydrogen as transportation fuel. *Appl Energy* 2011;88(12):4517–26.
- [16] Calise F, et al. A novel solar-geothermal trigeneration system integrating water desalination: Design, dynamic simulation and economic assessment. *Energy* 2016. 115;Part 3:1533–47.
- [17] Calise F, et al. A novel hybrid polygeneration system supplying energy and desalinated water by renewable sources in Pantelleria Island. *Energy* 2017.
- [18] Wang Z, et al. Optimal planning of a 100% renewable energy island supply system based on the integration of a concentrating solar power plant and desalination units. *Int J Electr Power Energy Syst* 2020;117:105707.
- [19] Karavas C-S, Arvanitis KG, Papadakis G. Optimal technical and economic configuration of photovoltaic powered reverse osmosis desalination systems operating in autonomous mode. *Desalination* 2019;466:97–106.
- [20] Mohan G, et al. A novel solar thermal polygeneration system for sustainable production of cooling, clean water and domestic hot water in United Arab Emirates: Dynamic simulation and economic evaluation. *Appl Energy* 2016;167:173–88.
- [21] Pfeifer A, Prebeg P, Duić N. Challenges and opportunities of zero emission shipping in smart islands: A study of zero emission ferry lines. *eTransportation* 2020;3:100048.
- [22] Dorotić H, et al. Integration of transport and energy sectors in island communities with 100% intermittent renewable energy sources. *Renew Sustain Energy Rev* 2019;99:109–24.
- [23] Pfeifer A, et al. Integration of renewable energy and demand response technologies in interconnected energy systems. *Energy* 2018;161:447–55.
- [24] Alves M, Segurado R, Costa M. On the road to 100% renewable energy systems in isolated islands. *Energy* 2020;198:117321.
- [25] Calise F, Dentice d'Accadida M, Piacentino A. A novel solar trigeneration system integrating PVT (photovoltaic/thermal collectors) and SW (seawater) desalination: Dynamical simulation and economic assessment. *Energy* 2014;67:129–48.
- [26] Klein SA, et al. Solar Energy Laboratory, TRNSYS. A transient system simulation program. Madison: University of Wisconsin; 2006.
- [27] Calise F, et al. Thermo-economic analysis of an integrated solar combined cycle power plant. *Energy Convers Manage* 2018;171:1038–51.
- [28] Murray, M.C., et al. Live Energy Trnsys -Trnsys Simulation within Google Sketchup. in Eleventh International IBPSA Conference. 2009. Glasgow, Scotland July 27–30.
- [29] Calise F. Thermoeconomic analysis and optimization of high efficiency solar heating and cooling systems for different Italian school buildings and climates. *Energy Build* 2010;42:992–1003.
- [30] Calise F, Vanoli L. Parabolic trough photovoltaic/thermal collectors: design and simulation model. *Energies* 2012;5:4186–208.
- [31] C. Richardson Chemical Engineering Volume Vol 2 5th Edition, 2002 Butterworth-Heinemann 2.
- [32] Wijmans JG, Baker RW. The solution-diffusion model: a review. *J Membr Sci* 1995;107(1):1–21.
- [33] Dimitriou E, et al. Theoretical performance prediction of a reverse osmosis desalination membrane element under variable operating conditions. *Desalination* 2017;419:70–8.
- [34] Gils HC, et al. GIS-based assessment of the district heating potential in the USA. *Energy* 2013;58:318–29.
- [35] Persson U, Werner S. Heat distribution and the future competitiveness of district heating. *Appl Energy* 2011;88(3):568–76.
- [36] Mulder M. Basic Principles of Membrane Technology. second edition Kluwer Academic Publishers; 2020.
- [37] Buonomano A, et al. A hybrid renewable system based on wind and solar energy coupled with an electrical storage: Dynamic simulation and economic assessment. *Energy* 2018;155:174–89.
- [38] Hoek EMV, et al. Modeling the effects of fouling on full-scale reverse osmosis processes. *J Membr Sci* 2008;314(1):33–49.
- [39] <https://global.aerme.com/it/>. 2018.
- [40] Bose A, et al. Co-production of power and urea from coal with CO₂ capture: performance assessment. *Clean Techn Environ Policy* 2015;1271–80.
- [41] Piacentino A, et al. Sustainable and cost-efficient energy supply and utilisation through innovative concepts and technologies at regional, urban and single-user scales. *Energy* 2019;182:254–68.
- [42] http://www.bigbrandwater.com/Dow-Filmtec-SW30ULE-440i-Seawater-Membrane_p_20550.html. 2019.
- [43] Du Y, et al. Optimization of reverse osmosis networks with split partial second pass design. *Desalination* 2015;365:365–80.
- [44] Olwig R, et al. Techno-economic analysis of combined concentrating solar power and desalination plant configurations in Israel and Jordan. *Desalin Water Treat* 2012;41:9–25.
- [45] Soltero VM, et al. Potential of biomass district heating systems in rural areas. *Energy* 2018;156:132–43.